Monthly Notices
of the
ROYAL ASTRONOMICAL SOCIETY

Mon. Not. R. Astron. Soc. **417,** 1510–1533 (2011) doi:10.1111/j.1365-2966.2011.19363.x

Herschel⋆-ATLAS: rapid evolution of dust in galaxies over the last 5 billion years

L. Dunne,[1]† H. L. Gomez,[2] E. da Cunha,[3,4] S. Charlot,[5] S. Dye,[2] S. Eales,[2] S. J. Maddox,[1] K. Rowlands,[1] D. J. B. Smith,[1] R. Auld,[2] M. Baes,[6] D. G. Bonfield,[7] N. Bourne,[1] S. Buttiglione,[8] A. Cava,[9] D. L. Clements,[10] K. E. K. Coppin,[11,12] A. Cooray,[13] A. Dariush,[2] G. de Zotti,[8,14] S. Driver,[15] J. Fritz,[6] J. Geach,[11,12] R. Hopwood,[13] E. Ibar,[16] R. J. Ivison,[16,17] M. J. Jarvis,[7] L. Kelvin,[15] E. Pascale,[2] M. Pohlen,[2] C. Popescu,[18] E. E. Rigby,[1] A. Robotham,[15] G. Rodighiero,[19] A. E. Sansom,[18] S. Serjeant,[20] P. Temi,[21] M. Thompson,[7] R. Tuffs,[22] P. van der Werf[16,23] and C. Vlahakis[24]

[1]*School of Physics & Astronomy, Nottingham University, University Park Campus, Nottingham NG7 2RD*
[2]*School of Physics & Astronomy, Cardiff University, Queen Buildings, The Parade, Cardiff CF24 3AA*
[3]*Max Planck Institute for Astronomy, Konigstuhl 17, 69117 Heidelberg, Germany*
[4]*Department of Physics, University of Crete, PO Box 2208, 71003 Heraklion, Greece*
[5]*Institut d'Astrophysique de Paris, CNRS, Université Pierre & Marie Curie, UMR 7095, 98 bis bd Arago, 75014 Paris, France*
[6]*Sterrenkundig Observatorium, Universiteit Gent, Krijgslaan 281 S9, B-9000 Gent, Belgium*
[7]*Centre for Astrophysics, Science & Technology Research Institute, University of Hertfordshire, Hatfield, Herts AL10 9AB*
[8]*INAF-Osservatorio Astronomico di Padova, Vicolo Osservatorio 5, I-35122 Padova, Italy*
[9]*Departmento de Astrofísica, Facultad de CC Físicas, Universidad Complutense de Madrid, E-28040 Madrid, Spain*
[10]*Department of Physics and Astronomy, University of California, Irvine, CA 92697, USA*
[11]*Department of Physics, McGill University, Ernest Rutherford Building, 3600 Rue University, Montreal, Quebec H3A 2T8, Canada*
[12]*Institute for Computational Cosmology, Durham University, South Road, Durham DH1 3LE*
[13]*Department of Physics, Imperial College, Prince Consort Road, London SW7 2AZ*
[14]*SISSA, Via Bonomea 265, I-34136 Trieste, Italy*
[15]*SUPA, School of Physics and Astronomy, University of St Andrews, North Haugh, St Andrews KY16 9SS*
[16]*UK Astronomy Technology Centre, Royal Observatory, Edinburgh EH9 3HJ*
[17]*SUPA, Institute for Astronomy, University of Edinburgh, Royal Observatory, Blackford Hill, Edinburgh EH9 3HJ*
[18]*Jeremiah Horrocks Institute, University of Central Lancashire, Preston PR1 2HE*
[19]*University of Padova, Department of Astronomy, Vicolo Osservatorio 3, I-35122 Padova, Italy*
[20]*Astrophysics Branch, NASA Ames Research Center, Mail Stop 2456, Moffett Field, CA 94035, USA*
[21]*Department of Physics and Astronomy, The Open University, Milton Keynes MK7 6AA*
[22]*Max Planck Institut für Kernphysik, Saupfercheckweg 1, D-69117 Heidelberg, Germany*
[23]*Leiden Observatory, Leiden University, PO Box 9513, NL-2300 RA Leiden, the Netherlands*
[24]*Departamento de Astronomia, Universidad de Chile, Casilla 36-D, Santiago, Chile*

Accepted 2011 June 30. Received 2011 June 30; in original form 2010 December 22

ABSTRACT

We present the first direct and unbiased measurement of the evolution of the dust mass function of galaxies over the past 5 billion years of cosmic history using data from the Science Demonstration Phase of the *Herschel*-Astrophysical Terahertz Large Area Survey (*Herschel*-ATLAS). The sample consists of galaxies selected at 250 μm which have reliable counterparts from the Sloan Digital Sky Survey (SDSS) at $z < 0.5$, and contains 1867 sources. Dust masses are calculated using both a single-temperature grey-body model for the spectral energy distribution and also a model with multiple temperature components. The dust temperature for either model shows no trend with redshift. Splitting the sample into bins of redshift reveals a

⋆*Herschel* is an ESA space observatory with science instruments provided by European-led Principal Investigator consortia and with important participation from NASA.

†E-mail: loretta.dunne@nottingham.ac.uk

strong evolution in the dust properties of the most massive galaxies. At $z = 0.4$–0.5, massive galaxies had dust masses about five times larger than in the local Universe. At the same time, the dust-to-stellar mass ratio was about three to four times larger, and the optical depth derived from fitting the UV-sub-mm data with an energy balance model was also higher. This increase in the dust content of massive galaxies at high redshift is difficult to explain using standard dust evolution models and requires a rapid gas consumption time-scale together with either a more top-heavy initial mass function (IMF), efficient mantle growth, less dust destruction or combinations of all three. This evolution in dust mass is likely to be associated with a change in overall interstellar medium mass, and points to an enhanced supply of fuel for star formation at earlier cosmic epochs.

Key words: ISM: evolution – galaxies: evolution – galaxies: ISM – submillimetre: galaxies.

1 INTRODUCTION

The evolution of the dust content of galaxies is an important and poorly understood topic. Dust is responsible for obscuring the UV and optical light from galaxies and thus introduces biases into our measures of galaxy properties based on their stellar light (Driver et al. 2007). The energy absorbed by dust is re-emitted at longer infrared and sub-millimetre (sub-mm) wavelengths, providing a means of recovering the stolen starlight. Dust emission is often used as an indicator of the current star formation rate (SFR) in galaxies – although this calibration makes the assumption that young, massive stars are the main source of heating for the dust and that the majority of the UV photons from the young stars are absorbed and re-radiated by dust (Kennicutt 1998; Kennicutt et al. 2009; Calzetti et al. 2007). Many surveys of dust emission from 24 to 850 μm (Saunders et al. 1990; Blain et al. 1999; Le Floc'h et al. 2005; Dye et al. 2010; Eales et al. 2010b; Gruppioni et al. 2010) have noted the very strong evolution present in these bands and this is usually ascribed to a decrease in the SFR density over the past 8 billion years of cosmic history ($z \sim 1$; Madau et al. 1995; Hopkins 2004). The interpretation of this evolution is complicated by the fact that the dust luminosity of a galaxy is a function of both the dust content and the temperature of the dust. It is pertinent to now ask the question '*What drives the evolution in the FIR luminosity density?*', is it an increase in dust heating [due to enhanced star formation (SF) activity] or an increase in the dust content of galaxies (due to their higher gas content in the past) – or both?

Dust is thought to be produced by both low–intermediate mass asymptotic giant branch (AGB) stars (Gehrz 1989; Ferrarotti & Gail 2006; Sargent et al. 2010) and massive stars when they explode as supernovae (SNe) at the end of their short lives (Rho et al. 2008; Dunne et al. 2009; Barlow et al. 2010). Thus, the dust mass in a galaxy should be related to its current and past SF history. Dust is also destroyed through astration and via SNe shocks (Jones et al. 1994), and may also reform through accretion in both the dense and diffuse interstellar medium (ISM; Tielens 1998; Inoue 2003; Zhukovska, Gail & Trieloff 2008). The life cycle of dust is thus a complicated process which many have attempted to model (Dwek 1998; Morgan & Edmunds 2003; Calura, Pipino & Matteucci 2008; Gall, Andersen & Hjorth 2011) and yet the basic statistic describing the dust content of galaxies – the dust mass function (DMF) – is not well determined.

The first attempts to measure the DMF were made by Dunne et al. (2000, hereafter D00) and Dunne & Eales (2001, hereafter DE01) as part of the SCUBA Local Universe Galaxy Survey (SLUGS) using a sample of *IRAS* bright galaxies observed with the Submillimeter Common User Bolometer Array (SCUBA) at 450 and 850 μm. Vlahakis, Dunne & Eales (2005, hereafter VDE05) improved on this by adding an optically selected sample with sub-mm observations. These combined studies, however, comprised less than 200 objects – none of which was selected on the basis of their dust mass. These studies were also at very low-z and did not allow for a determination of evolution. A high-z DMF was estimated by Dunne, Eales & Edmunds (2003a, hereafter DEE03) using data from deep sub-mm surveys. This showed considerable evolution with galaxies at the high-mass end requiring an order of magnitude more dust at $z \sim 2.5$ compared to today (for pure luminosity evolution), though with generous caveats due to the difficulties in making this measurement. Finally, Eales et al. (2009) used Balloon-borne Large Aperture Submillimeter Telescope (BLAST) data from 250 to 500 μm and also concluded that there was strong evolution in the DMF between $z = 0$ and 1 but were also limited by small number statistics and confusion in the BLAST data due to their large beam size.

In this paper, we present the first direct measurement of the space density of galaxies as a function of dust mass out to $z = 0.5$. Our sample is an order of magnitude larger than previous studies, and is the first which is near 'dust mass' selected. We then use this sample to study the evolution of dust mass in galaxies over the past ∼5 billion years of cosmic history in conjunction with the elementary dust evolution model of Edmunds (2001).

The new sample which allows us to study the DMF in this way comes from the *Herschel*-Astrophysical Terahertz Large Area Survey (H-ATLAS; Eales et al. 2010a), which is the largest open-time key project currently being carried out with the *Herschel* Space Observatory (Pilbratt et al. 2010). H-ATLAS will survey in excess of 550 deg^2 in five bands centred on 100, 160, 250, 350 and 500 μm, using the Photodetector Array Camera (PACS; Poglitsch et al. 2010) and Spectral and Photometric Imaging Receiver (SPIRE) instruments (Griffin et al. 2010). The observations consist of two scans in parallel mode reaching 5σ point source sensitivities of 132, 126, 32, 36 and 45 mJy in the 100, 160, 250, 350 and 500 μm bands, respectively, with beam sizes of approximately 9, 13, 18, 25 and 35 arcsec. The SPIRE and PACS map-making are described in the papers by Pascale et al. (2011) and Ibar et al. (2010), while the catalogues are described in Rigby et al. (2011). One of the primary aims of the H-ATLAS is to obtain the first unbiased survey of the local Universe at sub-mm wavelengths, and as a result was designed to overlap with existing large optical and infrared surveys. These Science Demonstration Phase (SDP) observations are centred on the 9^h field of the Galaxy And Mass Assembly (GAMA; Driver et al. 2011) survey. The SDP field covers 14.4 deg^2 and comprises approximately one thirtieth of the eventual full H-ATLAS sky coverage.

In Section 2, we describe the sample that we have chosen to use for this analysis and the completeness corrections required. In Section 3

we describe how we have derived luminosities and dust masses from the *Herschel* data, while in Section 4, we present the DMF and evaluate its evolution. Section 6 compares the DMF to models of dust evolution in order to explain the origin of the strong evolution. Throughout we use a cosmology with $\Omega_{\rm m} = 0.27$, $\Omega_\Lambda = 0.73$ and $H_0 = 71\,{\rm km\,s^{-1}\,Mpc^{-1}}$.

2 SAMPLE DEFINITIONS

The sub-mm catalogue used in this work is based on the $>5\sigma$ at 250 μm catalogue from Rigby et al. (2011), which contains 6610 sources. The 250 μm fluxes of sources selected in this way have been shown to be unaffected by flux boosting (see Rigby et al. 2011 for a thorough description). Sources from this catalogue are matched to optical counterparts from SDSS data release 7 (DR7) (Abazajian et al. 2009) down to a limiting magnitude of r-modelmag = 22.4 using a Likelihood Ratio (LR) technique (e.g. Sutherland & Saunders 1992). The method is described in detail in Smith et al. (2011a). Briefly, each optical galaxy within 10 arcsec of a 250 μm source is assigned a reliability, R, which is the probability that it is truly associated with the 250 μm emission. This method accounts for the possibility that true IDs are below the optical flux limit, the positional uncertainties of both samples, and deals with sharing the likelihoods when there are multiple counterparts. For our study we have used a reliability cut of $R \geq 0.8$ as this ensures a low contamination rate (<5 per cent), leaving 2423 250 μm sources with reliable counterparts. The LR method tells us that ∼3800 counterparts should be present in the SDSS catalogue; however we can only unambiguously associate around 64 per cent of these. Our sample is thus low in contamination but incomplete (we will deal specifically with the incompleteness of the ID process in the next section). A further cut was made to this sample to remove any stars or unresolved objects; this was done using a star–galaxy separation technique based on optical/IR colour and size, similar to that used by Baldry et al. (2010). Only six objects in the final reliable ID catalogue have 'stellar or quasi-stellar object (QSO) IDs' and so required removal. We also removed the five sources which were identified as being lensed by Negrello et al. (2010).

We then used the GAMA data base (Driver et al. 2011) to obtain spectroscopic redshifts for as many of the sources as possible (GAMA target selection is based on SDSS so no further matching is required). These are supplemented by public redshifts from SDSS DR7 (Abazajian et al. 2009), 2SLAQ-LRG (Cannon et al. 2006), 2SLAQ-QSO (Croom et al. 2009) and 6dFGRS (Jones et al. 2009). Where spectroscopic redshifts were not available we used photometric redshifts which were produced for H-ATLAS using SDSS and UKIDSS-LAS (Lawrence et al. 2007) data and the ANNz method (Collister & Lahav 2004). This method is described fully in Smith et al. (2011a).

Section 2.1 shows that we can quantify the statistical completeness of the IDs out to $z = 0.5$ and we choose this as the redshift limit of the current study. The total number of sources in the final sample is 1867 with 1095 spectroscopic redshifts. With this sample, the number of expected false IDs (summing $1 - R$; see Smith et al. 2011a) is 60 (or 3.2 per cent).

2.1 Completeness corrections

There are three sources of incompleteness in this current sample.

(i) *Sub-mm catalogue incompleteness* (C_s). This is due to the 250 μm flux limit of the survey and the efficacy of the source extraction process. The catalogue number density completeness has been estimated through simulations and presented by Rigby et al. (2011). Apart from the very small range of flux near to the limit, at 32–34 mJy, the catalogue is >80 per cent complete. Correction factors are applied to each source in turn, based on its flux, following tables 1 and 2 in Rigby et al. (2011). The largest correction is in the flux range 32–32.7 mJy and is a factor of 2.17; this applies to 124 sources out of a total of 1867 at $z < 0.5$.

Table 1. The percentage completeness of our reliable ID catalogue as a function of redshift, as taken from Smith et al. (2011a). The correction factor used in the LF is denoted by C_z.

z	Completeness (per cent)	C_z
0.0–0.1	93.2	1.07
0.1–0.2	83.2	1.20
0.2–0.3	74.2	1.35
0.3–0.4	55.6	1.80
0.4–0.5	53.1	1.88

(ii) *ID incompleteness* (C_z). The LR method measures in an empirical way a quantity Q_o, which is the fraction of SPIRE sources with counterparts above the flux limit in the optical survey. However, it is not possible to unambiguously identify all these counterparts with >80 per cent confidence due to positional uncertainties, close secondaries and the random probability of finding a background source within that search radius. Smith et al. (2011a) have estimated a completeness for reliable IDs as a function of redshift. This allows us to make a statistical number density correction in redshift slices for the sources which should have a counterpart above the SDSS limit in that redshift slice, but which do not have $R \geq 0.8$. This correction is applied to each source and is listed in Table 1. The ID incompleteness is a function of redshift (not unexpectedly) with corrections of a factor of ∼2 needing to be applied in the highest redshift bins.

(iii) *Optical catalogue incompleteness* (C_r). This correction is required because the SDSS catalogue from which we made the identifications is itself incomplete as we approach the optical flux limit of $r = 22.4$. We ascertained the completeness using the background source catalogue used in the ID analysis of Smith et al. (2011a), containing all sources which passed the star–galaxy separation at r-modelmag <22.4 in the primary SDSS DR7 catalogue in a region of ∼35° centred on the SDP field. We fitted a linear slope to the logarithmic number counts in the range $r = 19$–21.5 and extrapolated this to fainter magnitudes. We then used the difference between observed and expected number counts to estimate completeness. The results are presented in Table 2 and show that completeness is above 80 per cent to $r = 21.8$, falling to 50 per cent by $r = 22.2$. By restricting our analysis to $z < 0.5$ we keep 97 per cent of the sources below $r \sim 22$ and so in the range of acceptable completeness. It is possible, in principle, for there to be some form of optical incompleteness in the sample which is not corrected for with the above prescription, e.g. a population of objects which begin to appear at high redshifts in the H-ATLAS sample but which are not well represented in SDSS. Such a population could conceivably consist of very obscured starbursts. To test our susceptibility to this, we estimate the SDSS r magnitude of a highly obscured galaxy with a spectral energy distribution (SED) like that of Arp 220 ($A_v = 15$) at our 250 μm flux limit at the redshift limit of $z = 0.5$ and find that it would still be detected in our sample. Fig. 1 shows three different SED templates normalized to

Table 2. The percentage completeness as a function of r magnitude for the catalogue used to make the identifications to H-ATLAS sources. The correction factor used in the LF is denoted by C_r.

r-mag	Completeness (per cent)	C_r
21.6	91.1	1.10
21.7	87.6	1.14
21.8	82.8	1.21
21.9	77.7	1.29
22.0	70.5	1.42
22.1	61.6	1.62
22.2	52.5	1.90
22.3	42.8	2.33
22.4	17.0	5.88

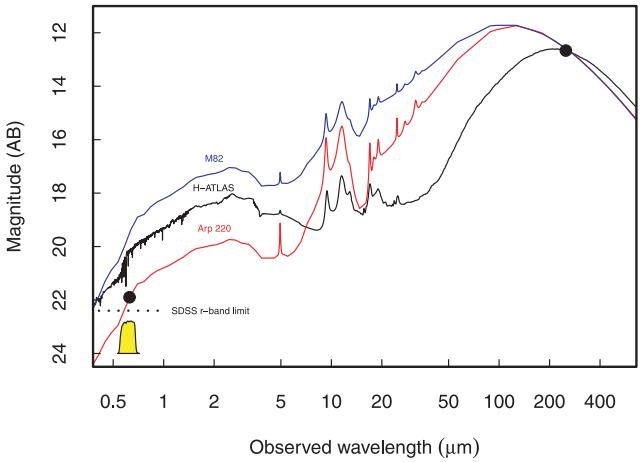

Figure 1. Templates for three galaxies showing the range of optical fluxes expected for galaxies which are at the SPIRE flux limit of $S_{250} = 32$ mJy at $z = 0.5$, the limit of our study. The templates are for M82 (a typical starburst), an H-ATLAS template derived from our survey data by Smith et al. (2011b), and Arp 220, a highly obscured local ultraluminous infrared galaxy (ULIRG). The SDSS limit of $r = 22.4$ is shown as a horizontal dotted line and even a galaxy as obscured as Arp 220 is still visible as an ID to our optical limit at $z = 0.5$. The yellow shape represents the SDSS-r-band filter which was used to compute the optical flux.

$S_{250} = 32$ mJy at $z = 0.5$: M82, an H-ATLAS-based template appropriate for sources at $z = 0.5$ from Smith et al. (2011b) and Arp 220. All templates less obscured than Arp 220 are easily visible at our optical flux limit. We will therefore proceed on the assumption that no such new populations exist below the optical limit in our highest z bins.

Fig. 2(a) plots r-mag as a function of 250 μm flux. A galaxy with S_{250} below ∼100 mJy can have a wide range of optical magnitude (r-mag = 16.5–22.0), and while optical magnitude is a strong function of redshift this is not the case for the sub-mm flux. Fig. 2(b) shows r-mag as a function of redshift for all galaxies in the GAMA 9-h (Driver et al. 2011) spectroscopic sample (cyan), as well as the reliable SPIRE IDs (black). This shows a lack of *Herschel* sources at the fainter magnitudes at low redshifts (i.e. the lowest absolute magnitudes or stellar masses).[1] It appears that H-ATLAS is less sensitive to low stellar mass galaxies than the SDSS (due to them having lower dust masses) and so only at high-z does the r-band limit preclude the identification of *Herschel* sources.

[1] The limit of GAMA is $r \sim 19$ which is brighter than the SDSS limit used for H-ATLAS IDs ($r \sim 22.4$).

3 DUST MASS AND LUMINOSITY

The *Herschel* fluxes are translated into monochromatic rest-frame 250 μm luminosities following

$$L_{250} = 4\pi D^2 (1+z)\, S_{250}\, K, \quad (1)$$

where L_{250} is in W Hz^{-1}, D is the comoving distance, S_{250} is the observed flux density at 250 μm and K is the K-correction which is given by

$$K = \left(\frac{\nu_{\rm obs}}{\nu_{\rm obs(1+z)}}\right)^{3+\beta} \frac{e^{(h\nu_{\rm obs(1+z)}/kT_{\rm iso})} - 1}{e^{(h\nu_{\rm obs}/kT_{\rm iso})} - 1}, \quad (2)$$

where $\nu_{\rm obs}$ is the observed frequency at 250 μm, $\nu_{\rm obs(1\,+z)}$ is the rest-frame frequency, and $T_{\rm iso}$ and β are the temperature and emissivity index describing the global SED shape.

In order to derive the values required for the K-correction, a simple grey-body SED of the form $S \propto \nu^{\beta} B(\nu, T)$ was fitted to the PACS and SPIRE fluxes as described in Dye et al. (2010), with a fixed dust emissivity index of $\beta = 1.5$ and a temperature range of 10–50 K. Where insufficient data points are available for the fit (300/1867), the median temperature of 26 K from the galaxies which could be fitted was used. With only SPIRE data on the Rayleigh–Jeans side of the SED (as is the case for most sources), only the combination of β and $T_{\rm iso}$ is well constrained, with the two parameters being inversely correlated by the fit; good fits are obtained with $\beta = 1.5$–2.0. These simple grey-body fits can be performed for the majority of sources and are accurate at representing the flux between rest-frame 250 and 166 μm (relevant for our redshift range) and so are suitable for applying the K-correction.

A dust mass can also be calculated from the observed 250 μm flux density and the grey-body temperature as

$$M_{\rm iso} = \frac{S_{250}\, D^2\, (1+z)\, K}{\kappa_{250}\, B(\nu_{250}, T_{\rm iso})}, \quad (3)$$

where κ_{250} is the dust mass absorption coefficient which we take to be equal to 0.89 m^2 kg^{-1} at 250 μm (equivalent to scaling $\kappa_{850} = 0.077$ m^2 kg^{-1}, as used by D00; James et al. 2002; da Cunha, Charlot & Elbaz 2008, hereafter DCE08, with a $\beta = 2$). It also lies within the range of values found for the diffuse ISM in the Milky Way and other nearby galaxies (Boulanger et al. 1996; Sodroski et al. 1997; Bianchi, Davies & Alton 1999; Planck Collaboration 2011a). The dust mass via equation (3) scales as $M_{\rm d} \propto T^{-2.4}$ at $z \sim 0$ for temperatures around 20 K; changing the temperature from 20 to 30 K results in a reduction in mass by a factor of 2.6. At $z = 0.5$ this dependence is steeper since the peak of the dust emission is shifted to longer wavelengths so the observed frame is even further from the Rayleigh–Jeans regime. Changing from $\beta = 1.5$ to 2.0 reduces the temperatures by ∼3K and increases the dust masses by ∼30–50 per cent.

This isothermal dust mass estimate can be biased low as it is now well established that dust exists at a range of temperatures in galaxies. Only dust in close proximity to sources of heating (e.g. star-forming regions) will be warm enough to emit at $\lambda \leq 100$ μm but this small fraction of dust (by mass) can strongly influence the temperature of the isothermal fits. The bulk of the ISM (and therefore the dust) resides in the diffuse phase which is heated by the interstellar radiation field to a cooler temperature typically in the range of 15–20 K (Helou 1986; DE01 and references within; Popescu et al. 2002; VDE05; Draine et al. 2007; Willmer et al. 2009; Bendo et al.

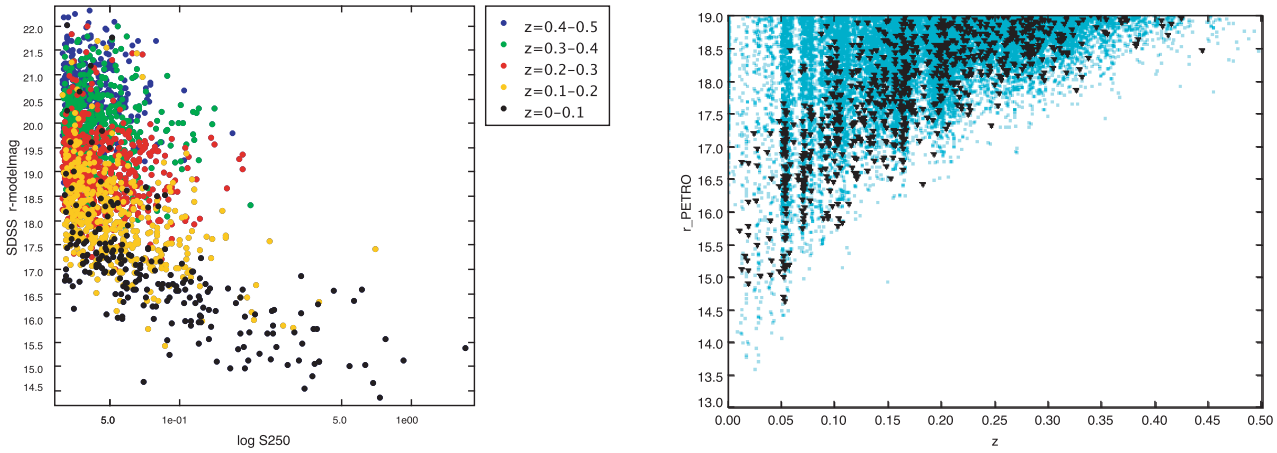

Figure 2. Left: SDSS *r*-modelmag as a function of 250 μm flux. There is no strong correlation apart from at the brightest fluxes. Only four galaxies lie within 0.4 mag of the flux limit used for IDs ($r < 22.4$) at $z < 0.5$ and so we consider that optical incompleteness is not a serious problem for this sample. Right: *r*-mag versus redshift for all sources in GAMA-9 (pale blue squares) and SPIRE IDs with $R \geq 0.8$ (black triangles). *Herschel* sources tend to be larger mass optical galaxies and so the SDSS flux-limit does not affect our ability to optically identify H-ATLAS sources until $z \sim 0.5$. Note that the right-hand panel uses the brighter limit of $r < 19$ appropriate for the GAMA redshift survey.

2010; Bernard et al. 2010; Boselli et al. 2010; Kramer et al. 2010; Planck Collaboration 2011b). For more accurate dust mass estimates we require the mass-weighted temperature of the dust emitting at 250 μm which requires fitting a model with multiple (at least two) temperature components. This is not to say that the FIR fluxes for most of the H-ATLAS galaxies are not fitted adequately by the single-temperature model; an isothermal model and a more realistic multi-temperature model are often degenerate in their ability to describe the SED shape with a limited number of data points. To illustrate this, we show in Fig. 3 an example of isothermal and two-component SED fits to an H-ATLAS source with a well-sampled SED. Although the two-component fit is formally better, there is nothing to choose between them as descriptions of the fluxes of the H-ATLAS source between 60–500 μm. DE01 studied this issue for a sample of SLUGS galaxies with 450 μm detections, and concluded that the best overall description of that sample was a two-temperature model with $\beta = 2$ and a cold component temperature of ∼20 K.

To deal with the cold dust component, we now introduce a more sophisticated SED model which includes dust in several physically motivated components, following the prescription of Charlot & Fall (2000). The results of this fitting are presented and described in detail in Smith et al. (2011b), and outlined here in brief. This simple, but empirically motivated, SED model fits broad-band photometry from the UV-sub-mm to estimate a wide variety of parameters (DCE08; da Cunha et al. 2010a). The method uses libraries of optical and infrared models (25 000 optical and 50 000 infrared) and fits those optical-IR combinations which satisfy an energy balance criteria to the data. The optical libraries have stochastic SF histories and the stellar outputs are computed using the latest version of the Bruzual & Charlot (2003) population synthesis code (Charlot & Bruzual, in preparation) libraries and a Chabrier (2003) Galactic-disc initial mass function (IMF).

The dust mass in this model is computed from the sum of the masses in various temperature components contributing to the SED, including cool dust in the diffuse ISM, warm dust in birth clouds, hot dust (transiently heated small grains emitting in the mid-IR) and polycyclic aromatic hydrocarbons (PAHs). In the fits to H-ATLAS sources (and SINGS galaxies; DCE08) around 90 per cent of the dust mass is in the cold diffuse ISM component and this is also the

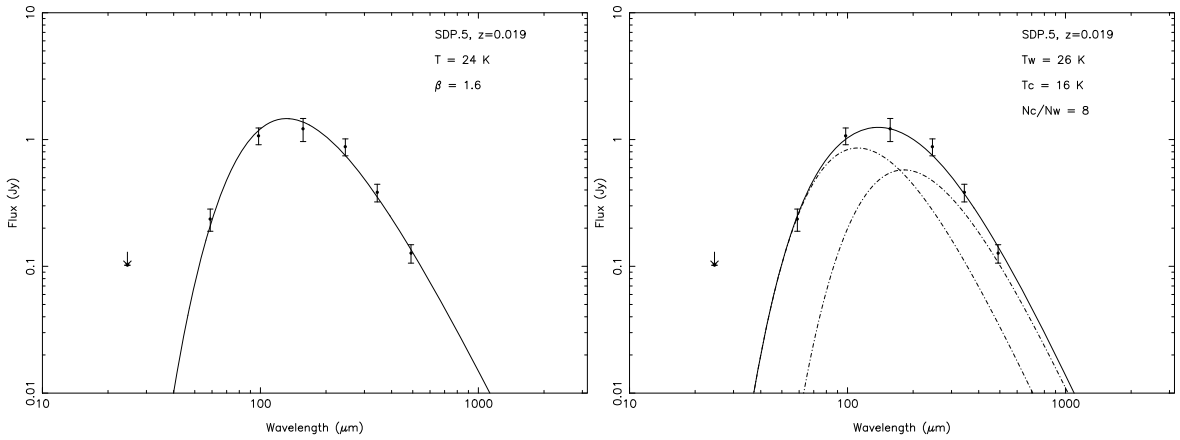

Figure 3. Top row: isothermal and two-component SEDs for an H-ATLAS sources with a well-sampled SED. Redshifts and fitted parameters are shown in each panel. For the isothermal fits T and β were free to vary while for the two-component fits β was fixed to be 2. The parameter N_c/N_w is the ratio of cold/warm mass.

best constrained component due to the better sampling of the FIR and sub-mm part of the SED with *Herschel*. Many other studies also find that the cold dust component dominates the overall mass, and so it is the most important one to constrain when measuring the DMF (e.g. DE01; VDE05; Draine et al. 2007; Willmer et al. 2009; Liu et al. 2010). The priors used by DCE08 for the temperatures of the grains in equilibrium are 30–60 K for the warm component and 15–25 K for the cold component. These values agree well with temperatures measured for local galaxies (Braine et al. 1997; Alton et al. 1998; Popescu et al. 2002; Hippelein et al. 2003; Meijerink et al. 2005; DE01; V05; Stevens, Amure & Gear 2005; Draine et al. 2007; Stickel, Klaas & Lemke 2007; Willmer et al. 2009; Planck Collaboration 2011b) and also with temperatures measured from stacking optically selected galaxies with the same stellar mass and redshift range as our sample into H-ATLAS maps (Bourne et al. 2011). The value of κ used in the DCE08 model is (by design) comparable with that used in the isothermal fits here.

The prior space of the parameters is sampled by fitting to several million optical–FIR model combinations and returns a probability density function (PDF) for the dust mass and other parameters (e.g. dust temperature, stellar mass, dust luminosity, optical depth and SFR) from which the median and 68 per cent confidence percentiles are taken as the estimate of the quantity and its error.

This model was fitted to the 60 per cent of the galaxies in our sample for which useful optical and NIR data were available from GAMA. We fitted only to galaxies which have matched aperture photometry in *r*-defined apertures as this best represents the total flux of the galaxy in each band as described in Hill et al. (2011) and Driver et al. (2011). The distribution of sources with and without these SED fits as a function of redshift is shown in Fig. 4. Those without fits dominate only in the highest redshift bin, from $z = 0.4$ to 0.5.

The errors on the dust mass range from ± 0.05 to 0.27 dex and this error budget includes all uncertainties in the fitting from flux errors to changes in temperature and contribution of the various dust components. Some typical SED fits and PDFs for the dust mass and cold temperature parameters are shown in Fig. 5. The dust mass is generally a well-constrained parameter of these model fits; the PDF is narrower when more IR wavelengths are available as the cold temperature is then better constrained.

A comparison of the isothermal dust masses ($M_{\rm iso}$) and the full SED-based masses ($M_{\rm sed}$) is shown in Fig. 6(a) and there is generally poor agreement between the two, with the scatter of a factor of 2–3 related to the difference between the temperature of the isothermal fit and that of the DCE08 model fit. This sensitivity is because at 250 μm we are near to the peak of the blackbody function for the cold temperatures appropriate to the bulk of the dust mass (15–20 K). At longer sub-mm wavelengths (such as 850 μm), this temperature sensitivity is less severe, but the choice of dust temperature used when estimating masses at rest wavelengths close to those of *Herschel* is clearly important.

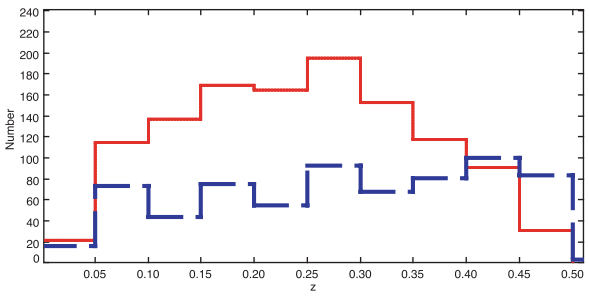

Figure 4. The distribution of sources with DCE08 SED fits as a function of redshift (red), and those without fits are shown in blue (dashed).

For sources which have insufficient UV-sub-mm data to use the DCE08 model, we need to extrapolate dust masses by comparing L_{250} with $M_{\rm sed}$ for those sources which do have fits. The relationship is linear, with some scatter introduced by the range in dust temperature for the cold ISM component (Fig. 6b):

$$\log M_{\rm sed} = \log L_{250} - 16.47. \quad (4)$$

Equation (4) is used to convert L_{250} to dust mass in cases where the full SED could not be fitted (747 sources out of 1867). The relationship between $M_{\rm sed}$ and the cold temperature of the diffuse ISM (which dominates the dust mass in these galaxies) is similar to that in equation (3), since the DCE08 model fits the sum of grey-bodies at different temperatures to the photometry. The colder the temperature fitted, the higher the dust mass will be for a given L_{250}. This is clearly demonstrated in Fig. 6(b). In using this relationship for sources without SED fits we are making the assumption that they will also fall on this relationship and that there is no systematic trend in those sources without fits (e.g. if only the highest redshift or most/least luminous sources did not have fits). Since the galaxies without fits span a range of redshift and luminosity and as we also find no correlation of temperature with L_{250} for our sample (see Section 4.2 and Fig. 14), there should be no bias introduced in using the relationship in Fig. 6(b) to estimate masses for those sources without fits.

The scatter in this figure is influenced by our choice of prior for the temperature of the diffuse dust component (15–25 K). Allowing a wider prior will broaden the scatter if a significant number of sources are best fitted by hotter or colder temperatures. This issue is explored further by Smith et al. (2011b) who conclude that for a sample of galaxies with well-constrained cold temperatures this prior encompasses >80 per cent of the population. Further study of the temperatures of the populations requires a larger sample with good five-band FIR/sub-mm photometry, which will be possible with the next phase of H-ATLAS data comprising 10 times the area of SDP. The difficulty in using a wider prior is that when we lack full coverage of the FIR/sub-mm SED (as is the case where we have only limits at PACS wavelengths and 500 μm) there is only a weak constraint on the cold temperature ($\sigma T_{\rm c} \sim 2.5$–3 K). This can place a galaxy with a real temperature of 15 K down at 12 K, and produces quite a bias in the fitted dust temperature (since at 12 K the mass is very sensitive to temperature). The model can fit arbitrarily high masses of very cold dust since this contributes little to the overall energy balance. Our choice to restrict the temperature prior to the parameter space which is preferred by observations of nearby galaxies, and by those galaxies well sampled in H-ATLAS, potentially means we underestimate the masses of some cooler sources, but we would prefer to be conservative at this point.

4 THE DUST MASS FUNCTION

4.1 Estimators

To calculate the DMF we use the method of Page & Carrera (2000, hereafter PC00) who describe a method to estimate binned luminosity functions (LF) that is less biased than the $1/V_{\rm max}$ method (Schmidt 1968). To begin with, we produce measurements of the 250 μm LF since this is more directly related to the flux measurements from *Herschel* and enables us to discuss the method without the added complication of translating 250 μm luminosity into dust

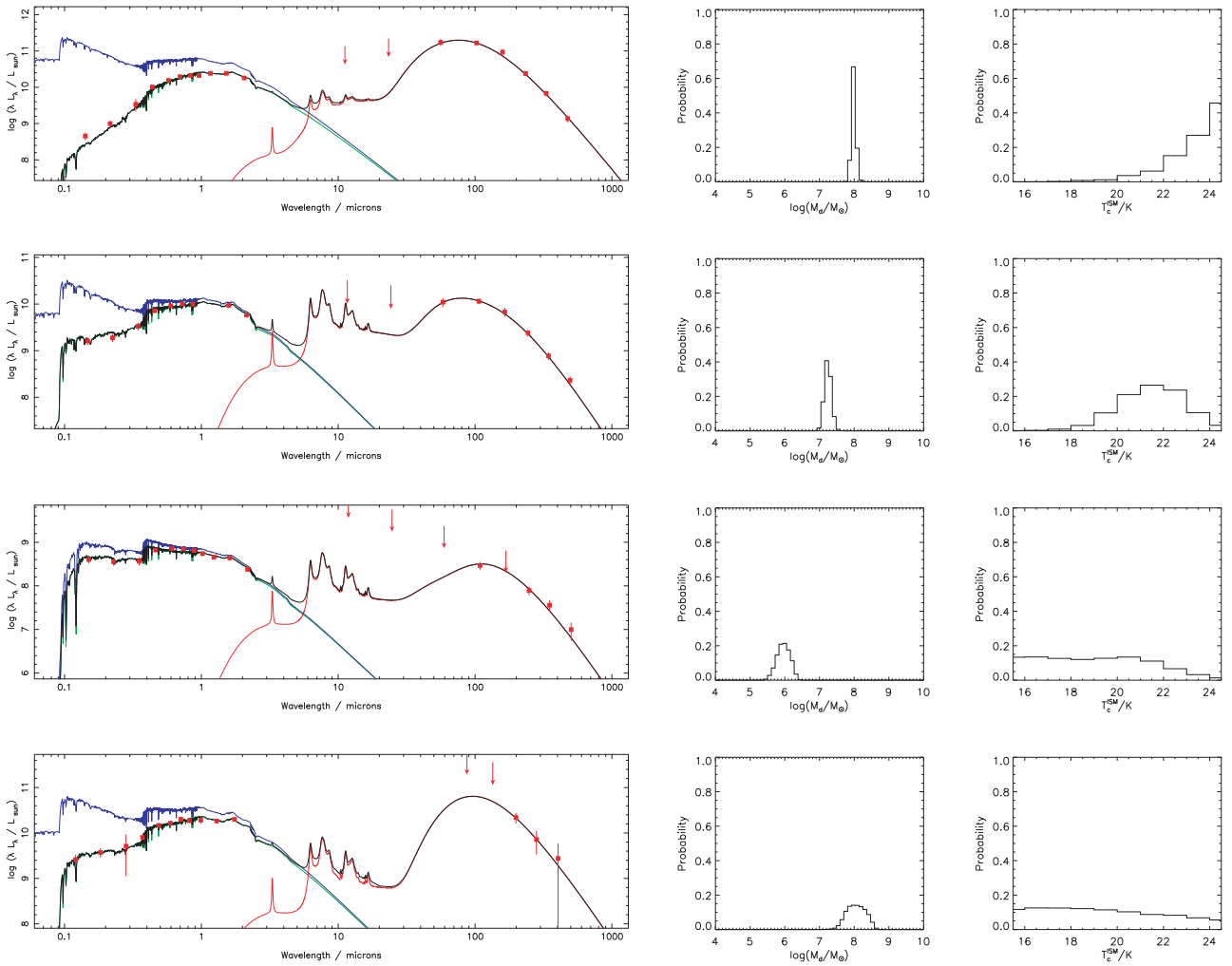

Figure 5. SED fits and probability distribution functions for dust mass and diffuse ISM dust temperature for a range of H-ATLAS sources. The black curve on the SED plot is the total attenuated starlight and re-radiated dust emission. Blue curve is the unattenuated starlight. Green is the attenuated starlight and red is the dust emission. The red squares show the observed photometry and errors or upper limits. The limit to the dust mass accuracy is our ability to determine the cold temperature, which is better constrained when there are more FIR data points available. The best constraints on the dust mass are ∼0.05 dex and the worst are ∼0.27 dex.

mass. The PC00 estimator is given by

$$\phi = \frac{\sum_{i=1}^{N} C_s\, C_z\, C_r}{\int_{L_{\rm min}}^{L_{\rm max}} \int_{z_{\rm min}}^{z_{\rm max}(L)} \frac{{\rm d}V}{{\rm d}z}\, {\rm d}z\, {\rm d}L} \tag{5}$$

where $C_s, C_z\, C_r$ are the completeness corrections for each object as described in Section 2.1 and the sum is over all galaxies in a given slice of redshift and luminosity bin. $L_{\rm max}$ and $L_{\rm min}$ are the maximum and minimum luminosities of the bin. $z_{\rm min}$ is the minimum redshift of the slice and $z_{{\rm max}(L)}$ is the maximum redshift to which an object with luminosity, L, can be observed given the flux limit and K-correction, or the redshift slice maximum, whichever is the smaller. The PC00 method has the advantage of properly calculating the available volume for each $L - z$ bin and, in particular, it does not overestimate the volume for objects near to the flux limit. This prevents the artificial turn-down produced by $1/V_{\rm max}$ in the first luminosity bin of each redshift slice. We compare to the $1/V_{\rm max}$ estimator in Fig. 7 and confirm that the $1/V_{\rm max}$ estimate of the 250 μm LF suffers from the bias noted by PC00 due to slicing in redshift bins.

In the PC00 formalism described above, the accessible volume is not calculated individually for each source (as for $1/V_{\rm max}$) but is instead calculated for each bin in the $L - z$ plane using a global K-correction. However, we know that each object in our sample has a different K-correction because they have different grey-body SED fits. We therefore modified the estimator such that the accessible volume for a given $L - z$ bin is calculated for each galaxy in that bin in turn using its grey-body SED fit to generate its limiting redshift $z_{{\rm max},i} = z(L_i, S_{\rm min}, T_{\rm d})$ across the bin. These individual contributions are then summed within the bin such that

$$\phi = \sum_{i=1}^{N} \frac{C_s\, C_z\, C_r}{\int_{L_{\rm min}}^{L_{\rm max}} \int_{z_{\rm min}}^{z_{{\rm max},i}} \frac{{\rm d}V}{{\rm d}z}\, {\rm d}z\, {\rm d}L}. \tag{6}$$

Note that this is not the same as reverting to the $1/V_{\rm max}$ estimator as we are still calculating the volume available for each $L - z$ bin; however we are now being more precise about the shape of the limiting curve for each source based on its individual SED. This is clear from the difference in the LF calculated this way, as shown in Fig. 7(b) compared to the PC00 and $1/V_{\rm max}$ methods shown in

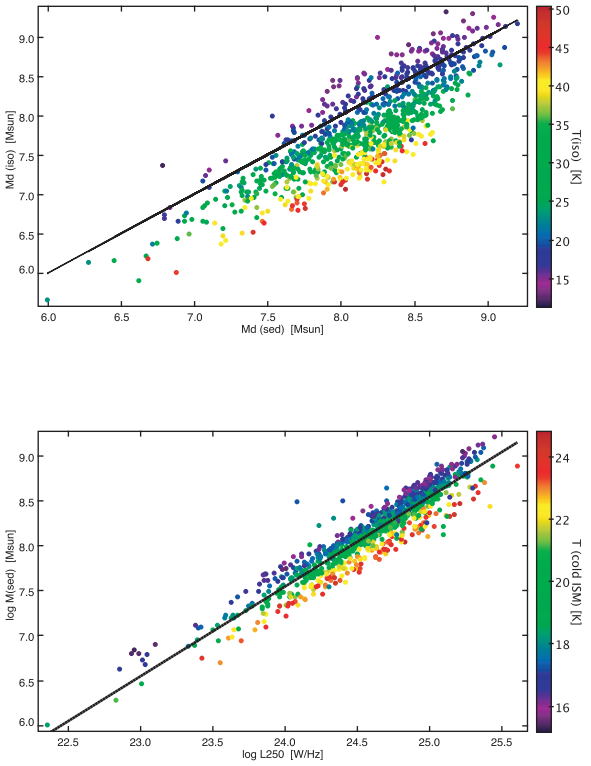

Figure 6. Top: comparison of dust masses from the DCE08 model ($M_{\rm sed}$) versus the dust mass obtained by using the isothermal grey-body fit ($M_{\rm iso}$) using equation (3). Points are colour-coded by the isothermal temperature. The one-to-one line is shown in black. There is a large difference between the two mass estimates which is a strong function of fitted isothermal temperature. Bottom: comparison of $M_{\rm sed}$ to L_{250} showing a reasonably tight and linear correlation. The best-fitting relationship (equation 4) is over-plotted. The scatter in this relationship is driven by the diffuse ISM dust temperature, which is used to colour-code the points.

Fig. 7(a). This change affected the highest redshift bins most as expected.

In this case, the error on the space density is given by

$$\sigma_\phi = \sqrt{\sum_{i=1}^{N} (\phi_i)^2}, \tag{7}$$

where ϕ_i is the individual ϕ contribution of a galaxy to a particular redshift and luminosity bin, and the sum is over all galaxies in that bin. The error bars in Fig. 7 show these errors.

This 250 μm LF differs slightly from that presented in Dye et al. (2010) in that the ID sample has since been updated to include extra redshifts (1867 compared to 1688) and also to remove stars, for which there were 130 contaminating the previous sample.[2] While Dye et al. (2010) did attempt to correct for incompleteness in the optical IDs of the sub-mm sample, we are now able to extend this to correct for incompleteness as a function of redshift, r-mag and sub-mm flux which was not previously possible. The results are, however, comparable in that strong evolution in the 250 μm LF is evident out to $z \sim 0.4$. There is then seemingly a halt, with little evolution between $z = 0.4$ and $z = 0.5$. This is still consistent with Dye et al. (2010) within the error bars of both estimators.

[2] Due to using an earlier version of the LR estimate which combined stars and galaxies together.

We suspect that this behaviour in the highest redshift bins is a result of a bias in the ANNz photo-z we are using. Fig. 8(a) shows a comparison between spectroscopic and photometric redshifts of H-ATLAS sources in the SDP region. There is a bias above $z \sim 0.3$–0.35 where the photometric redshifts tend to underestimate the true redshift (see Fleuren et al., in preparation). This issue is further exacerbated by the fact that this is also the redshift at which the LF becomes dominated by photo-z (Fig. 8b).

There is another potential bias in the highest-z slice due to the optical flux limit approaching the main body of galaxies in the sample. While we correct for the incompleteness in space density due to the r-band limit, we are not able to deal with any accompanying bias which might allow only those galaxies with lower dust-to-stellar mass ratios into the sample at the highest redshifts (see Fig. 19 and Section 6 for more discussion). Greater depth in optical/IR ancillary data will be required to test the continuing evolution of the luminosity and DMFs beyond $z = 0.5$ and this will soon be available with VISTA-VIKING and other deep optical imaging for the H-ATLAS regions currently underway.

Having demonstrated that our modified version of the PC00 estimator produces sensible results on the 250 μm LF, we now turn to the estimate of the DMF. We again use equation (6), however we now sum all galaxies in a bin of the $M_{\rm d} - z$ plane. We use the ratio of $M_{\rm d}$ to L_{250} to estimate the $L_{\rm max}$ and $L_{\rm min}$ for each galaxy, which is required to compute the individual K-correction. The results for both single-temperature masses and SED-based masses are shown in Fig. 9.

Both estimates of the DMF show a similar evolutionary trend as the 250 μm LF, with the same apparent slow down at higher redshift which we believe may be related to issues with the photo-z. The evolution is present whichever estimate of the dust mass is used; however, we will continue the discussion using the DMF from the DCE08 SED-based dust masses (Fig. 9a) as we believe that this is the best possible estimate at this time.

The DMF also shows a down-turn in some redshift slices at the low-mass end. We do not believe that this represents a true dearth of low-mass sources at higher redshifts but rather reflects the more complex selection function in dust mass compared to L_{250}. While there is a strong linear relationship between our dust mass and L_{250} (Fig. 6b) there is still scatter on this relationship due to the variation in the temperature of the cold dust in the ISM. At fixed L_{250}warm galaxies will have smaller dust masses than cooler ones, which leads to a sort of 'Eddington' bias in the dust masses. At the limiting L_{250} for a given redshift bin we are not as complete as we think for low dust masses, since we can only detect galaxies with low dust masses if their dust is warmer than average. This in turn leads to the apparent drop in space density. In the two highest redshift bins, the fraction of sources without SED fits increases and so the dust masses are then directly proportional to the 250 μm luminosity. To improve on this, we would need to use a bi-variate dust mass/L_{250} approach for which the current data are insufficient; however this analysis will be possible with the complete H-ATLAS data set.

4.2 Dust temperatures and evolution of the LF

An important ingredient in our estimate of the dust mass is the dust temperature. In order to interpret the increase in sub-mm luminosity as an increase in the dust content of galaxies, we have to be wary of potential biases in our measurements of the dust temperature. The dust temperature is most accurately constrained when PACS data, which span the peak of the dust SED, are available in conjunction with the longer sub-mm data from SPIRE, which also constrains the

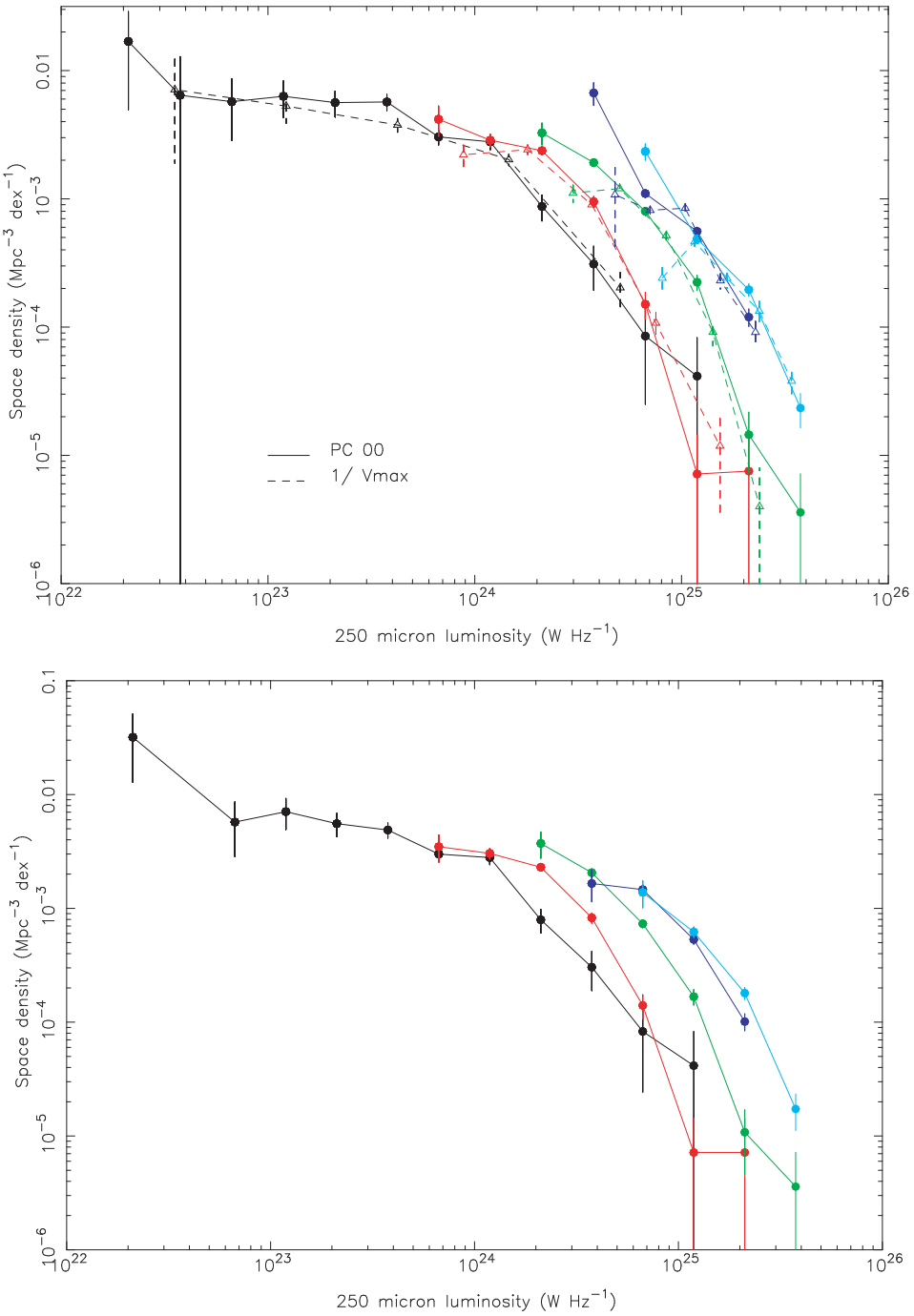

Figure 7. Top: 250 μm LFs calculated via the $1/V_{\rm max}$ method (open triangles/dashed) and PC00 method (solid circles and lines) in five redshift slices of $\Delta z = 0.1$ out to $z = 0.5$. Colours denote the redshifts as: black ($0 < z < 0.1$), red ($0.1 < z < 0.2$), green ($0.2 < z < 0.3$), blue ($0.3 < z < 0.4$) and cyan ($0.4 < z < 0.5$). The bias in $1/V_{\rm max}$ in the lowest luminosity bin in each redshift slice is apparent from the turn-down in this bin. Bottom: 250 μm LF calculated using the modified PC00 estimator which includes an individual K-correction for each object in an $L - z$ bin. Using individual K-corrections has a more significant effect in the highest redshift slices as expected.

cold temperature. For the SDP field, the PACS data are shallow and this results in PACS detections for only 262 galaxies. The fraction of PACS detections as a function of redshift are 41, 21, 8, 7, 4 per cent, respectively, from the lowest to highest redshift bin. A comparison of the temperatures from fits with PACS detections and without in the lowest redshift bin (where PACS samples a representative fraction of the population) is shown in Fig. 10. Fits without PACS detections are included only if the 350 μm flux was greater than 3σ in addition to the $>5\sigma$ 250 μm flux. The left-hand panel shows the cold dust temperature from the DCE08 fits and it can be seen that PACS sources have a range of cold ISM temperatures; however, those without PACS detections tend to have mostly cooler dust in their ISM. Smith et al. (2011b) show that the DCE08 fitting does tend to underestimate the cold temperature slightly when PACS data are removed from a fit, but this effect is of the order of $\sim$1 K and does not fully account for the difference in these distributions. When

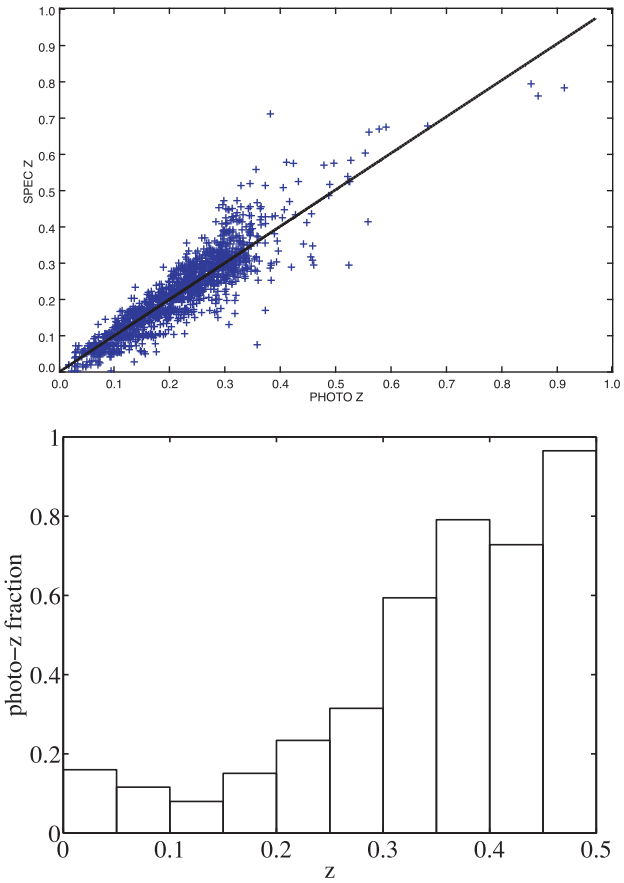

Figure 8. Top: comparison of spectroscopic versus photometric redshifts for galaxies in the H-ATLAS SDP. There is a bias in the photo-z at redshifts greater than $\sim$0.3 where photo-z tends to underestimate the true redshift. A one-to-one correlation is shown by the solid line. Bottom: the fraction of photo-z used in the LF as a function of redshift. Photo-z starts to dominate the LF at the same redshift where the photo-z bias begins.

we consider instead the peak temperature of the SED, that given by the isothermal fit (right-hand panel in Fig. 10), we see a different trend. Now the PACS detections are found only at the higher end of the temperature range while those without PACS detections span a wider range of temperature. There is no bias when the PACS data are removed from the fits (the temperatures vary randomly by $\sim \pm 3$ K when the PACS data are removed). The sources with the coldest isothermal temperatures ($T_{\rm iso} < 20$ K) are not detected by PACS, even in the lowest redshift bin, as they either do not contain enough warm dust or are not massive enough to be detected in our shallow PACS data. We also note that where PACS does not provide a $>5\sigma$ detection, we use the upper limit in the fitting which provides useful constraints on dust temperature for many more H-ATLAS sources.

The trend for PACS to detect the warmer sub-population of H-ATLAS sources becomes more pronounced at higher redshift, as the galaxies must be intrinsically more and more luminous to be detected by PACS. Fig. 11 shows the fitted temperature versus redshift for sources which are detected by PACS (black points) and those not detected by PACS but which have at least two good quality sub-mm points for the fit. If we used only the PACS detected sample, we would infer an evolution in dust temperature in this redshift range – but this is a selection bias due to the sensitivity of the PACS bands to warm dust and the shallow survey limit for PACS.

We can also look at the dust colour temperatures of the H-ATLAS sources in comparison to other samples without the complications of fitting models. In Fig. 12 we compare the FIR/sub-mm colours of the 35 H-ATLAS sources which have 60, 100 and 500 μm detections at $\geq 3\sigma$ with the colours of SLUGS galaxies from DE01 and VDE05 to see how these sub-mm selected sources compare to those selected at 60 μm from the *IRAS* Bright Galaxy Sample (BGS; Soifer et al. 1989) or in the optical. H-ATLAS fluxes at 60 μm are from the Imperial *IRAS*-FSC Redshift Catalogue (IIFSCz) of Wang & Rowan-Robinson (2009), 100 μm fluxes are from PACS and 500 μm from SPIRE (Rigby et al. 2011). To allow a comparison between 500 μm fluxes from H-ATLAS and 450 μm fluxes from SLUGS, we reduce the SLUGS 450 μm values by 37 per cent using a standard template suitable for SLUGS sources from DE01 (approximately $\propto \nu^3$ at these wavelengths). All of these sources are local. Fig. 12 shows that the H-ATLAS sources are significantly colder in their colours than the warmest end of the *IRAS* sample; they overlap rather better with the optically selected SLUGS sample. This is not surprising given our selection at 250 μm is more sensitive to the bulk dust mass of a galaxy while that at 60 μm from *IRAS* is more sensitive to warm dust (either large, warm grains in star-forming regions or small transiently heated grains). We note that, since only a very small number (35) of H-ATLAS sources are detected by *IRAS*, these few sources shown in Fig. 12 are also likely to have 'warmer' colours than the overall H-ATLAS sample. This agrees with the findings that PACS is sensitive to only the warmer H-ATLAS sources at higher redshifts and the SED fitting results which show that the H-ATLAS sources contain relatively cooler dust.

If the evolution in the 250 μm LF were due simply to an increase in the 'activity' of galaxies of the same dust mass, then we should see a corresponding increase in dust temperature with redshift and no evolution in the DMF. To explain the amount of evolution in the 250 μm LF without any increase in dust mass would require an increase in the average dust temperature of the order of a factor of 2 over the period $0 < z < 0.5$. We investigated the relationship between both the cold ISM dust temperature from the DCE08 fits and the isothermal grey-body temperature with redshift and found no trend for either (Fig. 13) at $z < 0.5$, similar to the results from Amblard et al. (2010) and inconsistent with the temperature evolution required to explain the increase in the 250 μm luminosity density.

The temperature of nearby ($z < 0.1$) dusty galaxies has been shown to be correlated with their IR luminosity (the so-called $L_{\rm ir}$–$T_{\rm d}$ relation; e.g. D00; Dale et al. 2001). A natural explanation for this observation might be that a galaxy which has hotter dust will have a larger IR luminosity than a similar mass galaxy with cooler dust. Recent work which extends to more sensitive surveys and samples selected at longer wavelengths suggests that this does not hold at higher redshifts and that galaxies are in general cooler at a given IR luminosity than previously believed (Coppin et al. 2008; Amblard et al. 2010; Rex et al. 2010; Symeonidis et al. 2009; Seymour et al. 2010; Smith et al. 2011b). Symeonidis, Page & Seymour (2011) suggest that this is due to more rapid evolution of 'cold' galaxies over the period $0.1 < z < 1$ than 'warm' ones. Recent studies at other wavelengths (70–160 μm from *Spitzer* and PACS) seem to support this interpretation, finding that cold galaxies are responsible for most of the increase in the IR luminosity density over the range $0 < z < 0.4$ (Gruppioni et al. 2010; Seymour et al. 2010). This is in agreement with the evolution seen in H-ATLAS galaxies which are largely this 'cold' population. Despite our average luminosity increasing with redshift, we see no increase in the average temperature

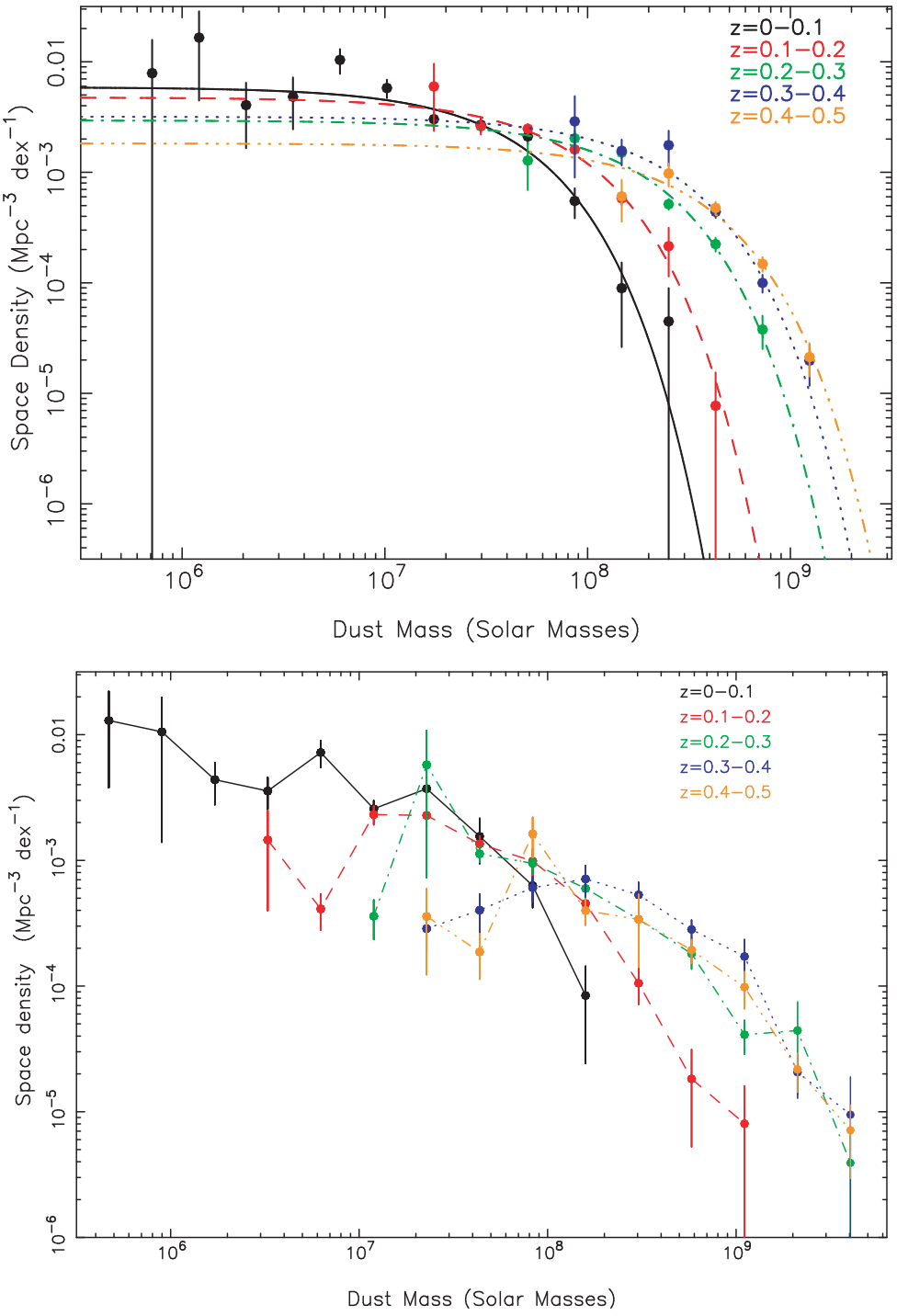

Figure 9. DMFs using the modified PC00 estimator calculated in five redshift slices of $\Delta z = 0.1$. Top: SED-based dust masses. Bottom: isothermal dust masses. The relation between dust mass and L_{250} has some scatter due to variation in the temperature of the cold ISM dust, which results in down-turns in the lowest mass bins in each redshift slice. The broader error on $M_{\rm d}$ acts to convolve the true DMF with a Gaussian of width approximately 0.2 dex. Schechter functions are plotted in the top panel with the faint-end slope fixed to that which fits best in the $z < 0.1$ slice. Parameters for the fits are given in Table 3.

(either isothermal or cold ISM temperature) and indeed we also see no correlation of either temperature with luminosity (either dust luminosity from the DCE08 model or L_{250}) for this sample (see Fig. 14).

To summarize, while we are subject to uncertainties in our ability to derive the dust masses and the exact scale of any evolution, we are nevertheless confident that:

(i) the evolution in the 250 μm LF out to $z = 0.5$ cannot be driven by dust temperature increases; there must be some evolution in the mass of dust as well.

(ii) the H-ATLAS sources at $z \leq 0.5$ are colder than previous samples based on *IRAS* data and therefore most of the evolution at low redshift is driven by an increase in the luminosity or space density of such cooler galaxies.

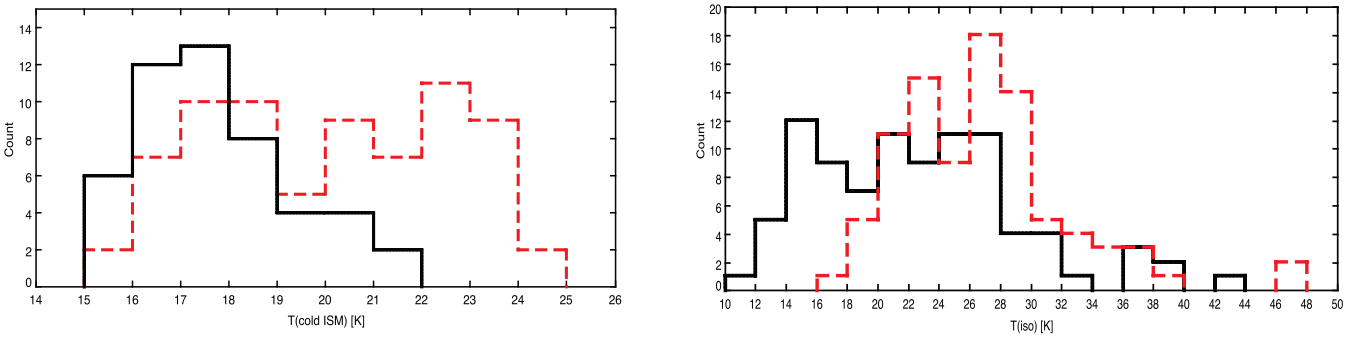

Figure 10. Left: cold ISM temperature from the DCE08 fits for the lowest redshift bin which has 41 per cent PACS detections. The sources with PACS detections are shown by the red dashed line while those without PACS detections but which do have a 350 μm flux above 3σ in addition to the 5σ 250 μm point are shown in black. Right: same but for the isothermal temperature.

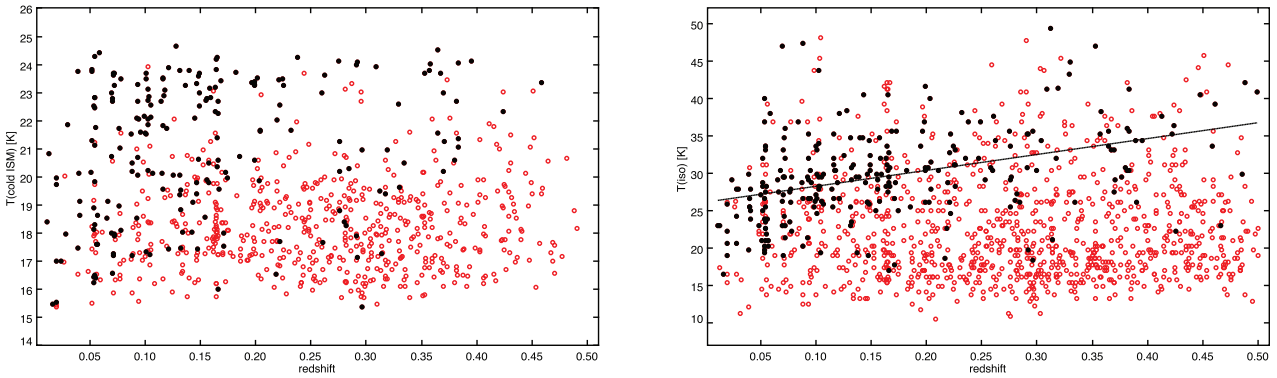

Figure 11. Left: cold ISM temperature from the DCE08 fits versus redshift for sources with PACS detections (black filled) and which have 350 μm fluxes above 3σ in additions to the 5σ 250 μm flux (red open). Right: same but for the isothermal temperature. Here there is a correlation between $T_{\rm iso}$ and redshift for the PACS detections ($r = 0.4$).

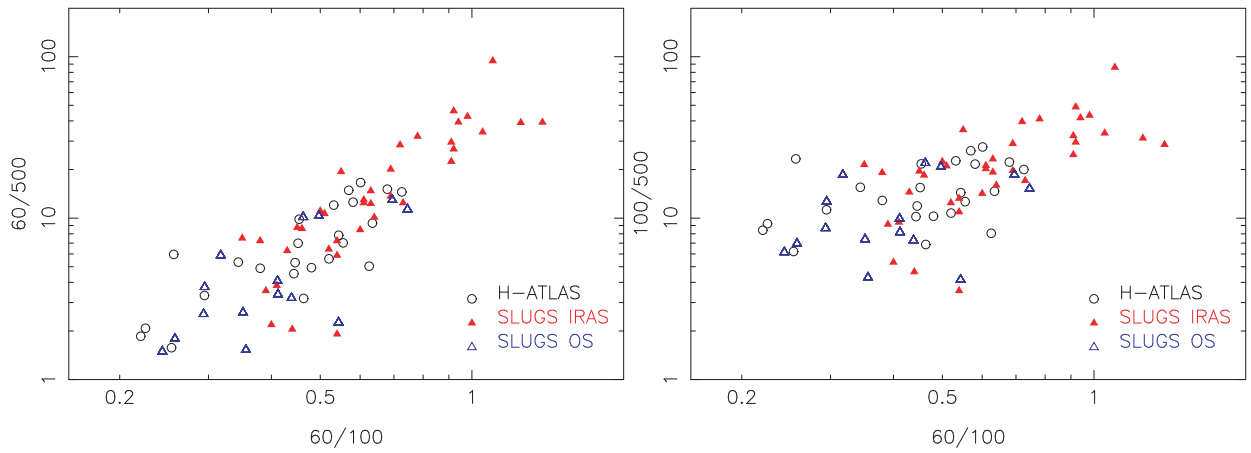

Figure 12. Colour plots for the 35 H-ATLAS galaxies with detections at 60, 100 and 500 μm compared to those for SLUGS sources detected at 450 μm from an *IRAS* 60 μm selected sample (*IRAS*) and an optically selected sample (OS). The SLUGS points have had their 450 μm fluxes adjusted downwards by 37 per cent to make them equivalent to 500 μm.

(iii) H-ATLAS sources show no trend of increase in dust temperature with either redshift or luminosity at $z < 0.5$

4.3 Comparison to low-redshift dust mass functions

We can compare the lowest redshift bin in the DMF ($0 < z < 0.1$) to previous estimates from SLUGS (D00; VDE05), which used SCUBA to observe samples of galaxies selected either at 60 μm from the *IRAS* BGS (Soifer et al. 1989) or in the *B* band from the Center for Astrophysics (CfA) redshift survey (Huchra et al. 1983). The *IRAS* SLUGS galaxies were mostly luminous starbursts, and in principle this should have produced an unbiased estimate of the local DMF as long as there was no class of galaxy unrepresented in the original *IRAS* BGS sample. However, it was argued in D00 and VDE05 that this selection at bright 60 μm fluxes quite likely missed cold but dusty galaxies, given the small sample size of ∼100, thus

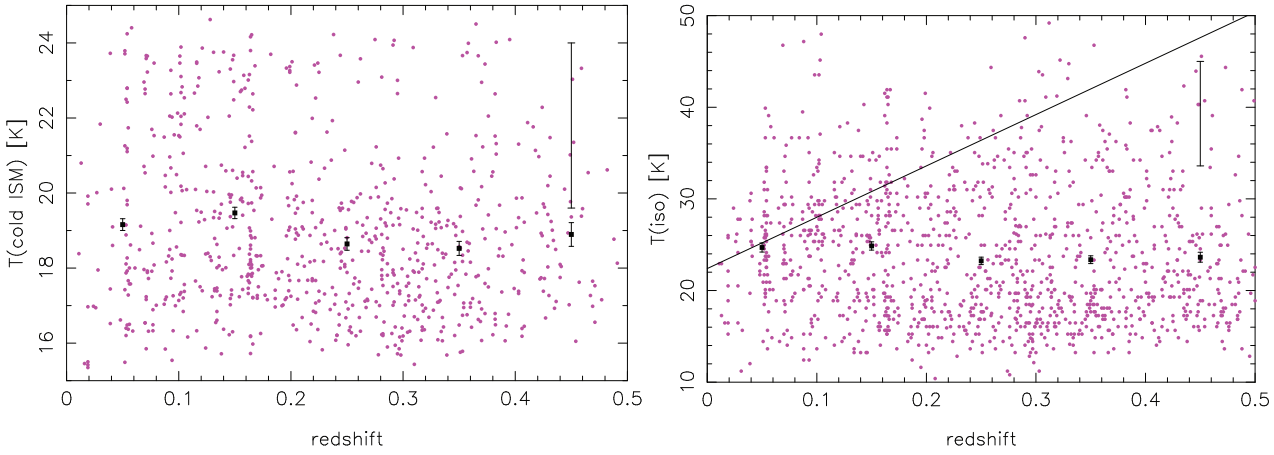

Figure 13. Left: the temperature of the cold interstellar dust component as a function of redshift z. Only sources with either a PACS detection or a 350 μm flux above 3σ, in addition to the 250 μm flux, are plotted. Mean values and 1σ errors on the mean are shown as black points. The data points in magenta show the full distribution of the temperatures. The large error bar in the top right shows the average 68 per cent confidence range on the temperature for an individual fit. Right: the isothermal temperature estimated from a grey-body fit versus redshift; same coding as before. The line plotted shows the evolution in temperature required in order to explain the evolution in the 250 μm LF *without* any increase in the dust masses. Neither method for estimating the dust temperature shows any evolution with redshift.

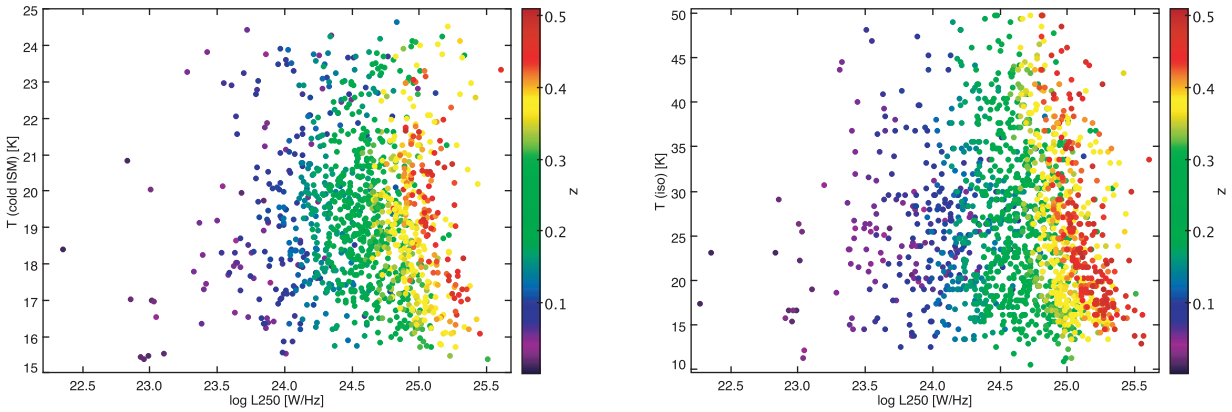

Figure 14. Left: cold dust temperature and L_{250} showing no correlation. The points are colour-coded by redshift. Right: same as (left) but for the isothermal dust temperature.

may have produced a DMF which was biased low. The optically selected SLUGS sample overcame the dust temperature bias and did indeed show that there were very dusty objects which were not represented as a class in the *IRAS* BGS (similarly confirmed by the *ISO* Serendipity Survey: Stickel et al. 2007). The directly measured DMF presented by VDE05 suffered from small number statistics, and instead V05 followed the work of Serjeant & Harrison (2005) in extrapolating the *IRAS* PSCz (Saunders et al. 2000) out to longer wavelengths (850 μm) using the empirical colour–colour relations derived from the combination of *IRAS* and optically selected SLUGS galaxies. This set of 850 μm estimates for all *IRAS* PSCz sources was then converted to a dust mass assuming a temperature of 20 K (the average cold component temperature found by DE01 and VDE05) and a mass opacity coefficient of $\kappa_{850} = 0.077\,\mathrm{m^2\,kg^{-1}}$. From this set of masses they then produced an estimate of the DMF.

The DMFs are compared in Fig. 15, where the black solid line and points are from H-ATLAS at $z < 0.1$, the blue dot–dashed line and filled triangles is the SLUGS *IRAS* directly measured DMF (D00) and the red dashed line and open triangles is the DMF based on the extrapolation of the *IRAS* PSCz by VDE05. In this figure, the H-ATLAS DMF has been corrected for the known underdensity of the GAMA 9-h field relative to SDSS as required when comparing to an all-sky measurement such as SLUGS or *IRAS* PSCz. This correction is a factor of 1.4 (Driver et al. 2011). The SLUGS DMFs have been corrected to the cosmology used in this paper; however these corrections are small at low-z.

It is remarkable that despite the considerable differences in sample size, area and selection wavelength, the SLUGS estimate from VDE05 based on extrapolating the *IRAS* PSCz gives a very good agreement to our measure. This implies that there is not a significant population of objects in the PSCz sample, or the H-ATLAS sample which is not represented by the combined optical and 60 μm selected SLUGS samples (which comprised only 200 objects). Note that had VDE05 used the *IRAS* data alone to measure dust masses, the results would be extremely different. SLUGS was only able to obtain such a good measure of the DMF due to their use of a cold temperature for the bulk of the dust mass, and their ability to make an empirical transition from *IRAS* colour to sub-mm flux.

The original direct measure of the DMF from the bright *IRAS* SLUGS sample (blue line in Fig 15; D00) dramatically underestimates the dust content in the local Universe (this was also noted by VDE05 once the optically selected sample was included).

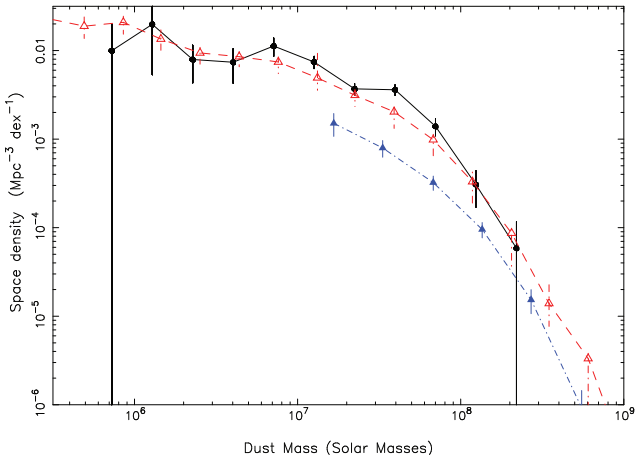

Figure 15. Comparison of the local DMFs at $z < 0.1$ from H-ATLAS (black solid line and points) along with estimates from SLUGS. Blue dot–dashed line and solid triangles – directly measured DMF from *IRAS* SLUGS sample (D00, DE01). Red dashed line and open triangles – extrapolated DMF from *IRAS* PSCz using sub-mm colours from the optical SLUGS sample (VDE05). The H-ATLAS points have been corrected for the factor of 1.4 under-density in the GAMA 9-h field for this redshift range compared to SDSS at large.

The dust masses were derived for those objects in an identical way to the VDE05 DMF (and very similar to our current method which has an average measured cold temperature of between 15 and 19 K); however the *IRAS* BGS simply missed objects which were dusty but did not have enough *warm* dust to make it above the 60 μm selection. *Herschel* is able to select sources based on their total dust content, rather than simply the small fraction of dust heated to >30 K. *Herschel* samples are therefore likely to contain a far wider range of galaxies in various states of activity, so long as they have enough material in their ISM.

4.4 Evolution of the dust mass function

For illustration, we now fit Schechter functions (Schechter 1976) to the DMFs in each redshift slice. Only in the first redshift bin do we fit to the faint end slope α, for other redshift bins we keep this parameter fixed at the value which best fits the lowest redshift bin ($\alpha = -1.01$) to avoid the incompleteness problem mentioned above with the lowest mass bins at high redshift. The best-fitting parameters for the slope α, characteristic mass $M_{\rm d}^*$ and normalization ϕ^* are given in Table 3, where the errors are calculated from the 68 per cent confidence interval from the χ^2 contours. For the lowest redshift bin, we include errors which reflect the marginalization over the unplotted parameter. The χ^2 contours for $M_{\rm d}^*$ and ϕ^* are shown in Fig. 16.

There is a strong evolution in the characteristic dust mass $M_{\rm d}^*$ with redshift, from $M^* = 3.8 \times 10^7\,{\rm M}_\odot$ at $z < 0.1$ to $M_{\rm d}^* = 3.0 \times 10^8\,{\rm M}_\odot$ at $z = 0.4$–0.5. There is seemingly a decline in ϕ^* over the same redshift range, from 0.0059 to 0.0018 Mpc^{-3} dex^{-1} (however this could also be due to sample incompleteness which is not corrected for despite our best attempts). The drop in ϕ^* and increase in $M_{\rm d}^*$ are correlated (see Fig. 16), and therefore we caution against using the increase in the fitted $M_{\rm d}^*$ alone as a measure of the dust mass evolution. If we keep ϕ^* fixed at 0.005 Mpc^{-3} dex^{-1} (which is the average of that for the first two redshift bins) then the $M_{\rm d}^*$ of the highest redshift bins decreases to $1.8 \times 10^8\,{\rm M}_\odot$ giving an evolution in $M_{\rm d}^*$ over the range $z = 0$–0.5 of a factor of ∼5 rather than ∼8 as is the case if the normalization is allowed to drop.

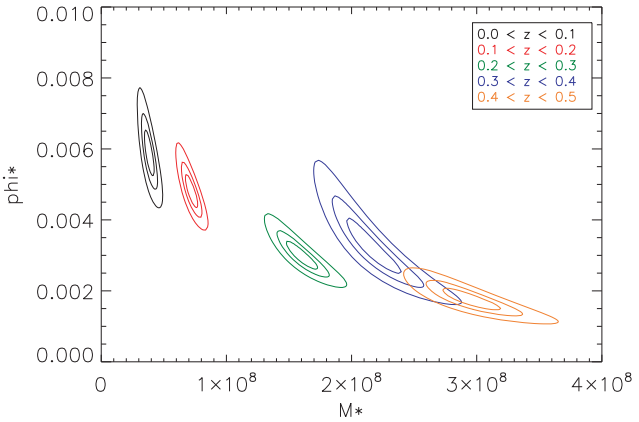

Figure 16. χ^2 confidence intervals at 68, 90, 99 per cent for $M_{\rm d}^*$ and ϕ^* with fixed α for the five redshift bins. This shows the clear evolution of $M_{\rm d}^*$ over the interval $0 < z < 0.5$.

Table 3. The Schechter parameters fitted to the DMF.

Redshift	α	$M_{\rm d}^*$ ($\times 10^7\,{\rm M}_\odot$)	ϕ^* ($\times 10^{-3}$ Mpc^{-3} dex^{-1})	$\rho_{\rm d}$ ($\times 10^5\,{\rm M}_\odot$ Mpc^{-3})	χ^2_ν	Cos. var.	$N_{\rm bin}$	$z_{\rm phot}/z_{\rm tot}$
0.0–0.1	$-1.01^{+0.17}_{-0.14}$	$3.83^{+0.73}_{-0.62}$	$5.87^{+1.38}_{-1.25}$		1.5	0.39	222	0.12
0.0–0.1	−1.01	$3.83^{+0.39}_{-0.43}$	$5.87^{+0.59}_{-0.62}$	0.98 ± 0.14	1.3	0.39	222	0.12
0.1–0.2	−1.01	$7.23^{+0.37}_{-0.45}$	$4.78^{+0.47}_{-0.41}$	1.51 ± 0.16	1.0	0.21	421	0.14
0.2–0.3	−1.01	$16.0^{+1.1}_{-1.2}$	$2.97^{+0.37}_{-0.34}$	2.08 ± 0.29	3.0	0.17	504	0.34
0.3–0.4	−1.01	$21.6^{+2.0}_{-1.8}$	$3.24^{+0.75}_{-0.74}$	3.06 ± 0.75	0.8	0.17	416	0.76
0.4–0.5	−1.01	$29.5^{+2.2}_{-2.0}$	$1.75^{+0.31}_{-0.27}$	2.26 ± 0.41	2.0	0.17	304	0.92
∼2.5	−1.08	39.1	1.74	3.11				

The first line of the table is the fit to all three parameters for the lowest redshift bin with associated errors from the 68 per cent confidence interval derived from the χ^2 contours. The following entries are where α is fixed to the best-fitting value in the lowest redshift bin. The final entry is the fit to the $z \sim 2.5$ DMF from DEE03 corrected to this cosmology and κ_{250}. Cos. var. is the cosmic variance estimated using the calculator from Driver & Robotham (2010). $N_{\rm bin}$ is the number of sources in that redshift bin and $z_{\rm phot}/z_{\rm tot}$ is the fraction of photometric redshifts in that bin.

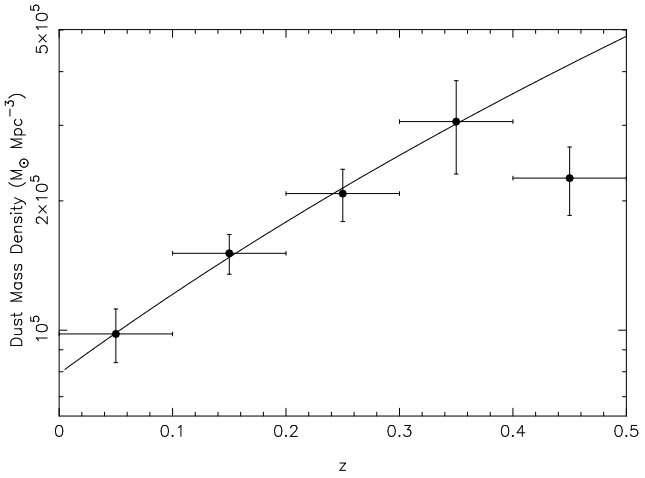

Figure 17. Integrated dust mass density as a function of redshift for H-ATLAS calculated using equation (8). The best-fitting relationship excluding the higher redshift point is over-plotted, which is $\rho_{\rm d} \propto (1+z)^{4.5}$.

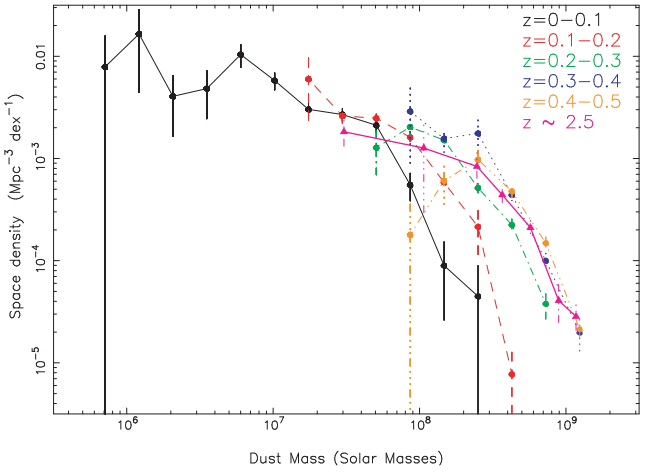

Figure 18. Comparison of the H-ATLAS DMF in five redshift slices (as in Fig. 9) and the high-redshift, $z \sim 2.5$, DMF from D03 (magenta dashed line).

We calculate the dust mass density in redshift slices using equation (8).

$$\rho_{\rm d} = \Gamma(2+\alpha)\, M_{\rm d}^{*}\, \phi^{*}. \quad (8)$$

This assumes that we can extrapolate the Schechter function beyond the range over which it has been directly measured. Given the low value of α used (~ -1), the resulting integral is convergent and so whether we extrapolate or not has negligible effect on the resulting mass density values. The values for $\rho_{\rm d}$ are listed in Table 3 and shown as a function of redshift in Fig. 17. There is clearly evolution in the cosmic dust mass density out to $z \sim 0.4$ of a factor of $\sim$3 which can be described by the relationship $\rho_{\rm d} \propto (1+z)^{4.5}$. In the highest redshift bin the dust mass density appears to drop (despite the increase in $M_{\rm d}^{*}$), but we again caution that this may be due to incompleteness/photo-z bias in the final redshift bin. This measure of the dust mass density at low redshift can be compared to that made by Driver et al. (2007). They used the optical B-band disc luminosity density from the Millennium Galaxy Catalogue scaled by a fixed dust mass-to-light ratio from Tuffs et al. (2004). Their quoted value for the dust density is $\rho_{\rm d} = 3.8 \pm 1.2 \times 10^5$ Mpc^{-3} at $z < 0.1$ but this is for a κ value from Li & Draine (2001) which is lower than that used here by 70 per cent. Scaling their result to our κ, and correcting the density of our lowest redshift bin by the factor of 1.4 from Driver et al. (2011) (to allow for the under-density of the GAMA 9-h field relative to SDSS at $z < 0.1$), we have values of $\rho_{\rm d} = 2.2 \pm 0.7 \times 10^5$ Mpc^{-3} (optical based) and $\rho_{\rm d} = 1.4 \pm 0.2 \times 10^5$ Mpc^{-3} (DMF) which are in rather good agreement given the very different ways in which these estimates have been made.

We can also calculate the dust mass density parameter $\Omega_{\rm dust}$ from

$$\Omega_{\rm dust} = \frac{\rho_{\rm d}}{\rho_{\rm crit}}$$

where $\rho_{\rm crit} = 1.399 \times 10^{11}\, {\rm M}_\odot$ Mpc^{-3} is the critical density for $h = 0.71$. This gives values of $\Omega_{\rm dust} = 0.7 - 2 \times 10^{-6}$ depending on redshift. Fukugita & Peebles (2004) estimated a theoretical value of $\Omega_{\rm dust} = 2.5 \times 10^{-6}$ today based on the estimated density of cold gas, the metallicity-weighted LF of galaxies and a dust to metals ratio of 0.2. This is a little higher than our (density corrected) lowest redshift estimate of $1.0 \pm 0.14 \times 10^{-6}$ but not worryingly so. Ménard et al. (2010) also estimate a dust density in the haloes of galaxies through a statistical measurement of reddening in background quasars when cross-correlated with SDSS galaxies. They estimate a dust density of $\Omega_{\rm dust}^{\rm halo} = 2.1 \times 10^{-6}$ for a mean redshift of $z \sim 0.35$ and suggest that this is dominated by $0.5\,L_{*}$ galaxy haloes. Comparing this to our measure of the dust *within* galaxies at the same redshift ($\Omega_{\rm dust}^{\rm gals} = 2 \times 10^{-6}$) we see that at this redshift there is about the same amount of dust outside galaxies in their haloes as there is within. We note here that dust in the haloes of galaxies will be so cold and diffuse that we will not be able to detect it in emission with H-ATLAS and so it is not included in our DMF. The decrease in $\rho_{\rm d}$ at recent times could be due to dust being depleted in SF, destroyed in galaxies by shocks or also lost from galaxies (and from our detection) to the haloes. We will return to this interesting observation in Section 6.

We can compare the DMF from H-ATLAS to that at even higher redshifts, as traced by the 850 μm selected submillimetre galaxy (SMG) population. An estimate of the DMF for these sources at a median redshift of $z \sim 2.5$ was presented in DEE03, using the $1/V_{\rm max}$ method. In Fig. 18 we show this higher-z DMF alongside the H-ATLAS data, where the $z \sim 2.5$ DMF is the magenta solid line with filled triangles. The DEE03 higher-z DMF has been scaled to the same cosmology and value of κ_{250} as used here. At $z \sim 2.5$, observed 850 μm corresponds to restframe $\sim$250 μm and so our lower-z H-ATLAS sample and the one at $z \sim 2.5$ are selected in a broadly similar restframe band. DEE03 used a dust temperature of 25 K to estimate the dust mass, which allowed for some evolution over the low-z SLUGS value of 20 K. The $z \sim 2.5$ sources from DEE03 are all ULIRGs and these higher luminosity sources do show enhanced dust temperatures in the local Universe (Clements, Dunne & Eales 2010; da Cunha et al. 2010b). It is also consistent with the cold, extended dust and gas component (T = 25–30 K) of the highly lensed SMG at $z = 2.3$ (Swinbank et al. 2010; Danielson et al. 2011) and other lensed sources discovered by *Herschel* (Negrello et al. 2010). If we were to recompute the $z \sim 2.5$ DMF using a temperature of 20 K instead, this would shift the points along the dust mass axis by a factor of $\sim$1.7.

For either temperature assumption, the $z \sim 2.5$ DMF is broadly consistent with the H-ATLAS DMF in the two highest redshift bins (z = 0.3–0.5). The fits to the high-z DMF are shown in Table 3 and the dust density at $z \sim 2.5$ is also consistent with that in the z = 0.3–0.5 range from H-ATLAS. If true, this implies that the rapid evolution in dust mass may be confined to the most recent 4–6 billion years of cosmic history. Notwithstanding the earlier statement that this trend needs to be confirmed with a larger sample, dust masses

are unlikely to continue rising at this pace because the dust masses at very high redshifts (Michałowski et al. 2010; Santini et al. 2010) are not very different to those we see here.

This implies that the evolution in the 250 μm LF is due at least in part to a larger interstellar dust content in galaxies in the past as compared to today, at least out to $z \sim 0.4$ (corresponding to a look-back time of 4 Gyr). However, an increase in SFR is also an important factor as if the dust mass increased at a constant SFR we would expect to see a decline in dust temperature with redshift. Our observations thus point to an increase in both dust mass and SF activity. If the evolution in the DMF is interpreted as pure luminosity (or mass) evolution (as opposed to number density evolution), then this corresponds to a factor of 4–5 increase in dust mass at the high-mass end over the past 4 Gyr. Since dust is strongly correlated to the rest of the mass in the ISM (particularly the molecular component), this also implies a similar increase in the gas masses over this period. In contrast, we know that the stellar masses of galaxies do not increase with look-back time, showing very little evolution in the mass range we are dealing with (predominantly L_* or higher) (Pozzetti et al. 2007; Wang & Jing 2010). The evolution of the DMF is therefore telling us something quite profound about the evolution of the dust content of galaxies, and by inference, the gas fractions of galaxies over this period.

5 THE DUST CONTENT OF H-ATLAS GALAXIES

There are two ways in which we can quantify the dust content: the amount of light absorbed by dust (or opacity), and the dust-to-stellar mass ratio. Both of these are derived from the DCE08 SED model fits for galaxies which were bright enough ($r \leq 20.5$) that aperture matched photometry was extracted by GAMA (Hill et al. 2011). Due to this being shallower than the depth to which we can ID the H-ATLAS sources we have to take care not to introduce selection biases when making these comparisons. Fig. 19 shows r-mag as a function of redshift for the H-ATLAS sources and again highlights that H-ATLAS does not detect low stellar mass (or low absolute M_r) sources. The panels in Fig. 19 have colour-coded points for sources where SED fits were made, and the colours represent either the V-band optical depth (top) or the dust-to-stellar mass ratio (bottom). At $z \sim 0.35$ the optical sample which has SED fits becomes incomplete, with only the brighter fraction of the galaxies having SED fits at a given redshift. This can lead to a lowering of the average optical depth, or dust-to-stellar mass ratio in bins at $z > 0.35$, since the brighter galaxies (higher stellar masses) tend to have lower values of optical depth or dust-to-stellar mass. Thus in the following discussion we limit our model comparisons to the data with $z < 0.35$. We hope to extend the SED fitting to the fainter sources in future work.

First, we plot the amount of optical light obscured by dust: the V-band opacity. This is derived from the DCE08 SED model fits, and is calculated both in the birth clouds where stars are born (τ_V from DCE08) and in the diffuse ISM ($\mu\tau_V$ from DCE08). Fig. 20 shows the evolution of both forms of V-band optical depth from the model fits, indicating that galaxies are becoming more obscured back to $z \sim 0.4$. Choi et al. (2006), Villar et al. (2008) and Garn et al. (2010) also find a higher dust attenuation in high-redshift star-forming galaxies. This is sometimes attributed to an increase of SFR with look-back time (Garn et al. 2010) and an attendant increase in dust content rather than to a change in dust properties. It is also possible that the apparent increase of optical depth with increasing redshift is related to the correlation between IR luminosity and dust attenuation (Choi et al. 2006), whereby more IR luminous galaxies tend to be more obscured. The average IR luminosity of our sample increases strongly with redshift (due to both the flux limit of the survey and the strong evolution of the LF) and it is currently not possible for us to disentangle the effects of redshift from those of luminosity since we do not have a large enough sample to make cuts in redshift at fixed luminosity. Regardless of which is the driver, the observational statement remains that a sub-mm selected sample will contain more highly attenuated galaxies at higher redshifts. This is in contrast to some UV selected samples which show either no trend with redshift or a decline of attenuation at higher-z, due to their selection effects (Burgarella et al. 2007; Xu et al. 2007; Buat et al. 2009). This just highlights the obvious – that FIR and UV selected samples are composed of quite different objects.

Our relationships with redshift are as follows:

$$\text{birth clouds}: \ \tau_V = 3.43z + 1.56$$

$$\text{diffuse ISM}: \ \mu\tau_V = 1.50z + 0.36,$$

which implies that the attenuation from the birth clouds is rising faster with increasing redshift than that in the diffuse ISM. At higher redshifts, we are therefore finding that the birth clouds are producing a larger fraction of the attenuation in the galaxy than at low redshift. We find this trend interesting but further work is required to explain and confirm it, first ensuring in a larger sample that it is not again related to the luminosity (more luminous sources also have higher relative attenuation from the birth clouds). Including Balmer line measurements in the DCE08 fits will also better constrain the optical depth in the birth clouds.

Secondly, we can look at dust and stellar mass together using the stellar masses from the DCE08 SED fits. Fig. 21 shows the variation of dust and stellar mass with redshift, where the dust mass has been scaled up by a factor of 178 in order to roughly make $M_{\rm d}$ and M_* equivalent at the lower boundary at low-z. Magenta points show stellar mass, open black squares are the scaled dust mass. The stellar mass remains fairly constant with redshift, while there is a distinct lack of high dust mass objects in the local Universe (as is shown also by the DMF). The dust-to-stellar mass ratio as a function of redshift is shown in Fig. 23 and discussed in more detail in the next section.

6 MODELLING THE EVOLUTION OF DUST

In this section, we will attempt to explain the evolution we see in the dust content of H-ATLAS sources and in the DMF. We do this using a chemical and dust evolution model which traces the yield of heavy elements and dust in a galaxy as its gas is converted into stars. A full treatment of the evolution of galaxies will be considered in Gomez et al. (in preparation). Here we will consider the elementary model of Edmunds (2001; see also Edmunds & Eales 1998) in which one assumes that the recycling of gas and dust in the ISM is instantaneous. Details of the model are given in Appendix A, but in brief, a galaxy is considered to be a closed box with no loss or addition of gas during its evolution. The evolution of the galaxy is measured in terms of f, its gas fraction, which represents the fraction of the baryonic mass in the form of gas. Gas is converted into stars using a SF prescription $\psi(t) = kg(t)^{1.5}$, where g is the gas mass and k is the SF efficiency (inversely proportional to the SF time-scale). We define an effective yield $p = p'/\alpha \sim 0.01$ where $\alpha \sim 0.7$ is the mass fraction of the ISM locked up in stars (equation A2) and p' is the yield returned from stars for a given IMF. We can interpret p as being the true mass fraction of heavy elements returned per stellar

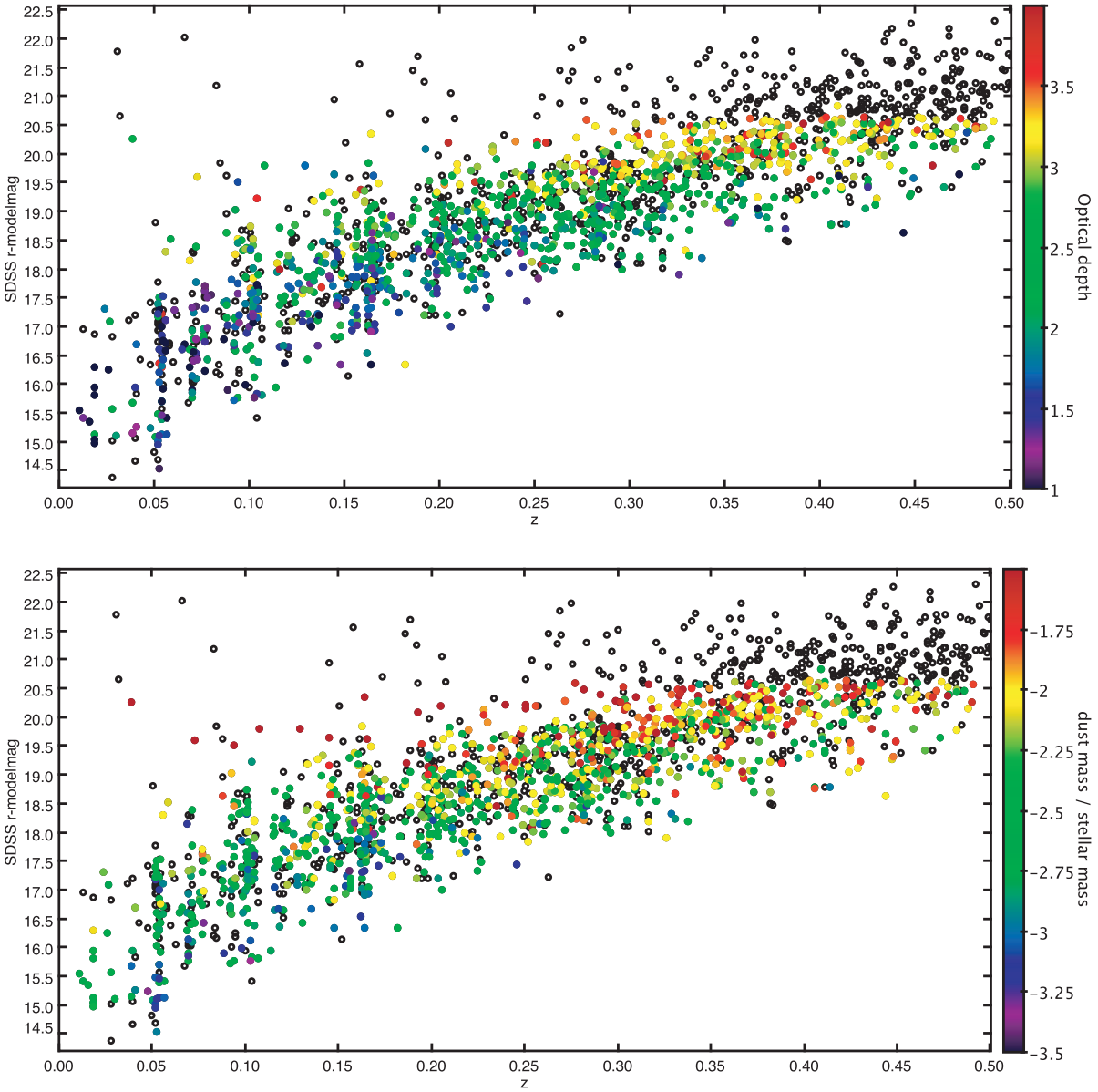

Figure 19. *r*-mag versus redshift for the H-ATLAS sources. Black open circles represent H-ATLAS sources which are too faint for an SED fit using the DCE08 model at the current time, or which were not in the region covered by GAMA photometric catalogues. Coloured points denote the values of either V-band optical depth (top) or dust-to-stellar mass ratio (bottom) from the DCE08 fits. The limit of reasonable completeness in the optical for the SED fits is $z \sim 0.35$. Beyond this redshift, averaged values of optical depth or dust-to-stellar mass ratio will be biased low because only the brightest optical galaxies in that redshift bin will have SED fits (and these tend to have less obscuration).

generation, since some fraction of the generated heavy elements is locked up in low-mass stars and remnants. In the first instance, we use the Scalo form of the IMF (Scalo 1986) for Milky Way evolution (e.g. Calura et al. 2008). The metal mass fraction of a galaxy is tracked through p and therefore follows metals incorporated into long lived stars and remnants or cycled through the ISM where they are available to be made into dust. The parameters which determine how many of the available metals are in the form of dust relate to the sources of dust in a galaxy and we consider three of these.

(i) Massive stars and SNe: χ_1 is the efficiency of dust condensation from new heavy elements made in massive star winds or SNe.

(ii) Low–intermediate mass stars (LIMS): χ_2 is the efficiency of dust condensation from the heavy elements made in the stellar winds of stars during their RG/AGB phases.

(iii) Mantle growth in the ISM: we can also assume that grains accrete at a rate proportional to the available metals and dust cores in dense interstellar clouds (Edmunds 2001). ϵ is the fraction of the ISM dense enough for mantle growth, and η_c is the efficiency of interstellar depletion in the dense cloud (i.e. if all the metals in the dense clouds are accreted on to dust grains then $\eta_c = 1$).

Morgan & Edmunds (2003) used observations of dust in LIMSs to show that $\chi_2 \sim 0.16$ yet theoretical models following grain growth in stellar atmospheres (e.g. Zhukovska et al. 2008) suggest higher values of $\chi_2 \sim 0.5$. We adopt the higher value here, but note that there is some considerable uncertainty on χ_2. For core-collapse SNe

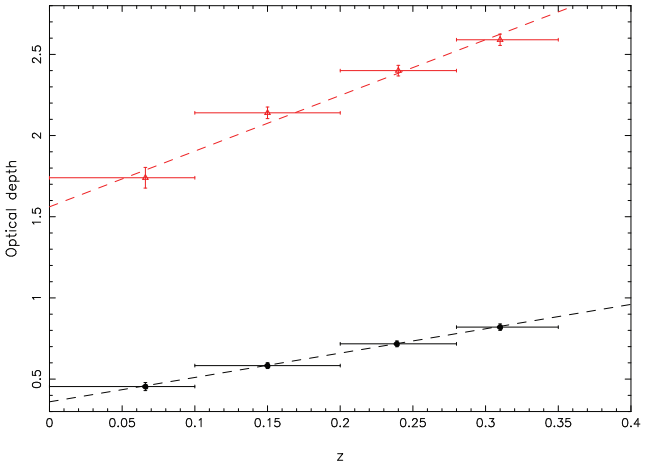

Figure 20. Upper red points: mean V-band optical depth in the birth clouds (from the DCE08 SED fits of Smith et al. 2011b) as a function of redshift with the best linear fit. Lower black points: V-band optical depth in the ISM ($\mu\tau_v$ from DCE08).

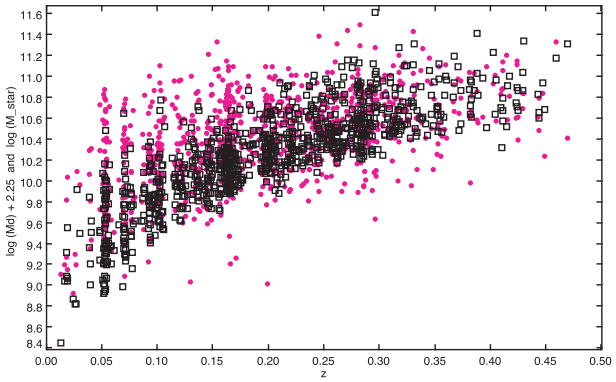

Figure 21. Stellar mass (magenta) and dust mass scaled by 178 (black open squares) versus redshift. The dust mass is scaled to make the dust and stellar lower limits approximately coincide at low-z. This illustrates the different trends of dust and stellar mass with redshift, with the dust mass evolving more rapidly than the stellar mass (as is also evident from the DMF). At lower redshifts there are many galaxies with higher stellar masses than the scaled dust mass, while at high redshifts both stellar and dust masses are comparable with the same scaling.

(using theoretical models of dust formation; e.g. Todini & Ferrara 2001) Morgan & Edmunds suggest that $\chi_1 \sim 0.2$; this agrees with the highest range of dust masses published for Galactic SN remnants (Dunne et al. 2003b, 2009; Morgan et al. 2003; Gomez et al. 2009). If core-collapse SNe are not significant producers of dust (e.g. Barlow et al. 2010) or if most of their dust is then destroyed in the remnant (Bianchi & Schneider 2007) then this fraction decreases to $\chi_1 \leq 0.1$, making it difficult to explain the dust masses we see in our Galaxy or in high-redshift sub-mm bright galaxies with stellar sources of dust (e.g. Morgan & Edmunds 2003; Dwek, Galliano & Jones 2007; Michałowski et al. 2010).

For mantles we arbitrarily set $\epsilon = 0.3$ and from interstellar depletion levels in our Galaxy and following Edmunds (2001), we set $\eta_c \sim 0.7$ (i.e. we assume that if the clouds are dense, then it is likely that the dust grains accrete mantles). In this scenario, the dust is formed during the later stages of stellar evolution and uses up the available metals in dense clouds. The addition of accretion of metals on to grain cores with the parameters described here will double the peak dust mass reached by a galaxy. Assuming no destruction of grains, a closed box model and mantle growth gives the highest dust mass attainable for galaxies.

Dust destruction can be added to this elementary model by assuming some fraction δ of interstellar grains are removed from the ISM as a mass ds is forming stars. We use two destruction scenarios: one with a constant destruction rate $\delta = 0.3$ (Edmunds 2001) and the second where δ is proportional to the Type-II SNe rate (which gives a similar result to Dwek's approximation for Milky Way (MW) IMF; Dwek & Cherchneff 2011). We also allow a mantle growth proportional to SFR since one would expect that the efficiency will depend on the molecular fraction of the ISM (which in turn is related to the SFR; Papadopoulos & Pelupessy 2010).

Finally, we relax the closed-box assumption and include outflows in the model (Appendix A) since galactic-scale outflows are thought to be ubiquitous in galaxies (Ménard et al. 2010 made a remarkable detection of dust reddening in the haloes of galaxies which implies at least as much dust is residing in the haloes as in the discs). Here, we test outflows in which enriched gas is lost at a rate proportional to one and four times the SFR (more powerful outflows are unlikely, since in the latter case, the galaxy would only retain approximately 20 per cent of its initial gas mass).

6.1 Evolution of dust-to-stellar mass

The dust-to-stellar mass ratio of the models discussed here is shown in Fig. 22 over the lifetime of the galaxy as measured by the gas fraction, f. The shaded region shows the range of values of M_d/M_* estimated for the H-ATLAS galaxies, which have a peak value of 7×10^{-3} at $z = 0.31$ and then decreases as the galaxy evolves in time (to lower gas fractions) to 2×10^{-3}. This global trend is reproduced by the closed box model where dust is contributed by *both* massive stars and LIMS, or via mantle growth; however the models struggle to produce values of M_d/M_* as high as observed. We also plot in Fig. 22 the variation of M_d/M_* if low–intermediate mass star-dust is the only stellar contributor to the dust budget ($\chi_1 = 0$, $\chi_2 = 0.5$). It is clear that the LIMS dust source cannot reproduce

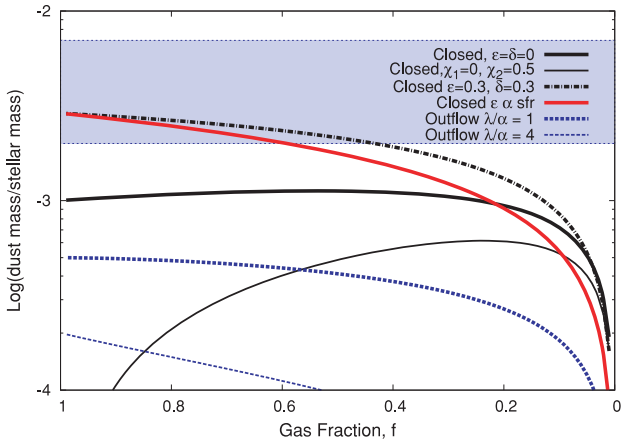

Figure 22. Variation of dust-to-stellar mass ratio as a function of gas fraction. The shaded box region is the range of values observed for the H-ATLAS galaxies. The models are (i) a closed box with no gas entering/leaving the system with dust from both SNe $\chi_1 = 0.1$ and LIMS stars $\chi_2 = 0.5$ (thick solid; black); (ii) with dust from LIMS only $\chi_1 = 0$, $\chi_2 = 0.5$ (thin solid; black); (iii) model (i) now including mantle growth (dot–dashed; black). (iv) A model with mantle growth, where the mantle rate is proportional to the SFR (solid; red); (v) and (vi) a model which has outflow with gas lost at a rate proportional to one or four times the SFR (λ/α) (dashed; blue).

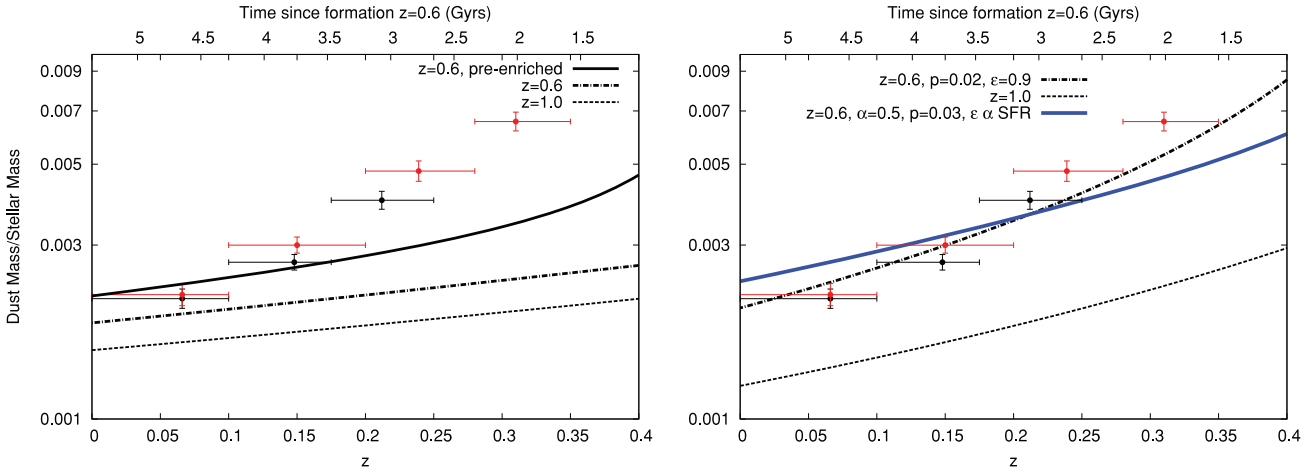

Figure 23. Left: the dust-to-stellar mass ratio as a function of redshift. Stellar and dust masses are derived from the SED fits using the models of DCE08 and are discussed in detail in Section 3 and Smith et al. (2011b). Black points show those sources with spectroscopic redshifts, while red points include photometric redshifts. Each sample is limited in redshift to the point where the optical flux limit is not biasing the selection to low dust-to-mass ratios. The model lines for the dust model (Section 6.1) corresponding to the Milky Way including mantle growth and destruction are over-plotted with formation redshifts of $z = 0.6$ (dot–dashed) and $z = 1$ (dotted). A model including pre-enrichment of $Z_i \sim 0.1\,Z_\odot$ with formation time-scale at $z = 0.6$ is also shown (solid; black). Right: same as left including pre-enrichment, but models are now tuned to match the data for the $z = 0.6$ formation time. With pre-enrichment, we require $\chi_1 = 0.1$, $\chi_2 = 0.5$, $p = 0.02$, $\epsilon = 0.9$ and SF efficiency $k = 1.5\,\mathrm{Gyr}^{-1}$ to 'fit' the data points (black dot–dashed) or $\chi_1 = \chi_2 = \epsilon = 0.5$, $p = 0.02$ (not shown). Also shown is a model with mantle growth varying with SFR and a top-heavy IMF described by $\alpha = 0.5, p = 0.03$ (solid; blue). Adding outflow or destruction rates which vary with SFR would make the decline in $M_\mathrm{d}/\mathrm{M}_*$ more pronounced at lower redshifts (later evolutionary times).

the values of dust/stellar mass seen in the H-ATLAS sources alone. Either significantly more dust is contributed to the ISM via massive stars/SNe than currently inferred, or a significant contribution from accretion of mantles in the ISM is required (indeed we would need significantly more dust accretion in the ISM than dust produced by LIMS). The simple model also suggests that the H-ATLAS galaxies must be gas rich ($f > 0.4$) in order to have dust-to-stellar mass ratios this high. (Typical gas fractions for spiral galaxies today are $f \sim 0.1$–0.2.)

We can also consider the evolution of dust-to-stellar mass as a function of time (equation A13). This is shown in Fig. 23(a) using dust production and yield parameters appropriate for spiral galaxies like the Milky Way ($p = 0.01, \alpha = 0.7, \chi_1 = 0.1, \chi_2 = 0.5, \epsilon\eta_\mathrm{c} = 0.24, k = 0.25\,\mathrm{Gyr}^{-1}$). We compare the model for two formation times of $z = 0.6$ and $z = 1$, where formation time in this model can simply mean the time of the last major SF event. In this scenario, we would expect any previous SF to have already pre-enriched the ISM with some metallicity Z_i, therefore increasing the available metals for grain growth in the ISM.

From Fig. 23(a), we see that the MW model does not match the variation of dust/stellar mass from H-ATLAS observations even if we increase the mantle growth or the amount of dust formed by stars, since the increase in dust-to-stellar content with gas fraction (as we look back to larger redshifts and earlier times in the evolution of the galaxy) is simply not rapid enough. Fig. 23(b) shows the same two formation times but now we have tuned the parameters to match the data for a formation at $z = 0.6$. In order to do this we have to increase the SF efficiency parameter ($k = 1.5\,\mathrm{Gyr}^{-1}$) to produce a steeper relationship as observed. An increase in k compared to the MW model is hardly surprising, since these higher values are typical of star-forming spirals with initial SFRs[3] of $\psi \sim 50\,\mathrm{M}_\odot\,\mathrm{yr}^{-1}$ which is in agreement with the observations of H-ATLAS sources at higher redshifts. However, increasing k then dramatically reduces the actual dust content at any epoch due to the removal of the ISM through the increase in SF efficiency. To explain the high M_d/M_* values for the H-ATLAS sample, we would then need to increase the dust condensation efficiencies (i.e. the amount of metals which end up in dust) to a minimum of 60 per cent and the effective yield p of heavy elements from stars would need increase by at least a factor of 2. This is much higher than observed condensation efficiencies for LIMS or massive stars/SNe although the difference could come from mantle growth. An increase in the effective yield can only be achieved through the IMF. The stellar masses of H-ATLAS galaxies are based on the Chabrier IMF (Chabrier 2003), which has $\alpha \sim 0.6$ (compared to $\alpha \sim 0.7$ for Scalo). However, to significantly increase the yield from the stellar populations, we would require a top-heavy IMF (e.g. Harayama, Eisenhauer & Martins 2008). In comparison to the MW-Scalo IMF, the effective yield p can increase by a factor of 4 and more material is returned to the ISM ($\alpha < 0.5$). A model with these 'top-heavy' parameters is shown in Fig. 23(b) (solid blue), and reproduces the H-ATLAS observations without the need for extremely efficient mantle growth or higher dust contribution from SNe. A top-heavy IMF also frees up more gas and metals in the ISM throughout the evolution of the galaxy with time, i.e. $f \sim 0.5$ at $z = 0.4$ compared to the $f \sim 0.3$ for a Scalo IMF, providing a consistent picture with the observed high dust-to-stellar mass ratios and the expected high gas fraction for H-ATLAS sources.

If we assume an earlier formation time, or time since last SF phase, the model cannot reproduce the H-ATLAS observations and would require even more extreme values for the dust condensation efficiency and/or yield. This suggests a time for the last major SF episode for H-ATLAS galaxies to be somewhere in the past 5–6 Gyr (which is consistent with the detailed SED modelling of Rowlands et al. 2011).

In summary, from this simple model, it is difficult to explain the high dust-to-stellar mass ratios in the H-ATLAS data even by assuming we are observing these galaxies at their peak dust mass unless (i) the fraction of metals incorporated into dust is higher

[3] Depending on the initial gas mass of the galaxies.

(although we would require $\chi > 70$ per cent of all metals to be incorporated into dust) or $\chi > 50$ per cent with pre-enrichment. (ii) The yield is significantly increased via a top heavy IMF. An IMF of the form $\phi(m) \propto m^{-1.7}$ would increase the yield and hence dust mass by a factor of 4, easily accounting for the highest M_d/M_* ratios. Such IMFs have been postulated to explain observations of high-z sub-mm galaxies, highly star-forming galaxies in the local Universe and galaxies with high molecular gas densities (Baugh et al. 2005; Papadopoulos 2010; Gunawardhana et al. 2011). (iii) H-ATLAS galaxies are rapidly consuming their gas following a relatively recent major episode of SF (at $z \sim 0.6$).

6.2 Evolution of the DMF

We now turn to the evolution of the dust mass itself as evidenced from the DMF (Fig. 9) which shows an increase in the dust mass of the most massive sources of a factor of 4–5 in a relatively small time-scale ($0 < z < 0.5$, $\Delta t < 5$ Gyr). To show the maximum change in dust mass in galaxies in the model, we plot the ratio (R) of dust mass at time t to that at the present day, assuming a gas fraction of $f \sim 0.1$ today (Fig. 24). For a closed box model, there is little evidence for the dust mass in a given galaxy changing by more than a factor of 1.5 in the past compared to its present-day value.

It is clear that including outflows produces a better fit to the variation of dust mass observed in the DMF, with the maximum change in dust mass approaching the observed change in DMF with $R \sim 4$ for the extreme outflow model. However, in this case, the peak M_d/M_* is at least an order of magnitude below the observed values predicting only 2×10^{-4} (see Fig. 22). In this scenario, we would require $\chi > 0.8$, $\epsilon\eta > 0.8$ and $p > 0.03$. Such high dust condensation efficiencies from stellar sources are not observed in the MW, and a yield as high as $p = 0.03$ would again imply a top heavy IMF. For an outflow model with $\lambda/\alpha = 1.0$, the parameters $\chi > 0.6$, $\epsilon\eta > 0.3$ and $p > 0.02$ would be required to produce the H-ATLAS dust-to-stellar mass ratios; these are more reasonable values yet this outflow rate is not sufficient to account for the increase in dust mass seen in the DMF (reaching a maximum $R \sim 1.5$; Fig. 24). We believe that outflows must be present at some level (Alton, Bianchi & Davies 1999) and the observation made earlier that there is as much dust in galaxy haloes as there is in galaxies themselves is strong circumstantial evidence for some outflow activity. Given that there are other ways (e.g. radiation pressure on grains; Davies et al. 1998) to remove dust from discs, we can attempt to derive a rough upper limit for the outflow required to produce as much dust in haloes at $z \sim 0.35$ as found by Ménard et al. (2010). We integrate the dust mass lost from outflows during the evolution of the galaxy and compare this to the dust mass in the galaxy at $z = 0.3$–0.4 for various values of outflow and SF efficiency k. The results are shown in Table 4. This assumes no dust destruction in either the halo or the disc, and as such is a very simple model. Equality in dust mass inside and outside galaxies can be achieved by $z = 0.3$ by having moderate outflow $<4 \times$ SFR and $0.25 < k < 1.5$ Gyr^{-1}. This is not to say that all galaxies need have similar evolution; it is quite likely that H-ATLAS sources are more active and dusty and as such may contain more dust in their haloes than the average SDSS galaxy probed by Ménard. This simple exercise merely gives some idea of what sort of 'average' chemical evolution history is required to reproduce the observation.

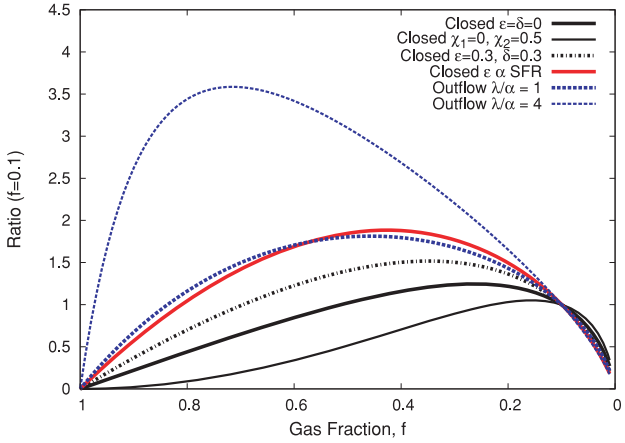

Figure 24. Ratio (R) of dust mass at gas fraction f to that at $f = 0.1$ (today). The models are (i) a closed box with no gas entering/leaving the system with dust from both SNe $\chi_1 = 0.1$ and LIMS stars $\chi_2 = 0.5$ (thick solid; black); (ii) with dust from LIMS only $\chi_1 = 0$, $\chi_2 = 0.5$ (thin solid; black); (iii) including mantle growth (dot–dashed; black). (iv) A model with mantle growth proportional to the SFR (solid; red); (v) and (vi) a model which has outflow with gas lost at a rate proportional to one or four times the SFR (λ/α) (dotted; blue). It is worth noting that for higher returned fraction from stars to the ISM (i.e. $\alpha = 0.5$), the ratio decreases for all models ($R < 3$ for the extreme outflow).

Table 4. t is the age since formation of the galaxy at $z = 0.6$. Outflow = 1 and 4 is outflow proportional to 1 and 4 times the SFR. 'Halo/disc' is the ratio of the integrated dust mass lost in outflow from t_{form} to t divided by the dust mass in the galaxy at t.

z	t (Gyr)	Outflow = 1 $k = 0.25$ Gyr^{-1} halo/disc	Outflow = 1 $k = 1.5$ Gyr^{-1} halo/disc	Outflow = 4 $k = 0.25$ Gyr^{-1} halo/disc
0.5	0.5	0.09	0.42	0.33
0.4	1.0	0.2	0.96	0.73
0.3	2.2	0.4	3.03	1.95
0.2	3.2	0.5	5.47	3.24
0.1	3.5	0.6	12.2	5.13

We now have a conundrum in that the observed evolution in dust mass requires significant outflow of material; however such outflow leads to the lowest values of dust-to-stellar mass ratio and cannot be reconciled to the observations without extreme alterations to the condensation efficiencies for dust or the stellar yields. Including dust destruction and mantle growth models which vary with the SFR alleviates this somewhat since both decrease the dust mass more significantly at later times. The change in dust mass over the same period compared to the elementary model with constant ϵ and δ is then more pronounced, but not enough to explain the evolution in the DMF.

One solution to this is if the galaxies with the highest dust masses at $z \sim 0.4$–0.5 are not the progenitors of the H-ATLAS sources at $z \sim 0.1$. We speculate on a scenario where the low-redshift spiral galaxies ($z < 0.15$) which do fit the MW model in Fig. 23(a) comprise one population and the higher redshift (more dusty) objects are a rapidly evolving starburst population with much higher SF efficiencies (higher k), higher dust condensation efficiencies and/or top-heavy IMFs. The fate of the high-redshift dusty population is that they rapidly consume their gas (and dust) in SF and by low redshift they are no longer detected in H-ATLAS as their gas and dust is exhausted ($f < 0.05$). Today they would lie in the faint end of the DMF, mostly below the limits to which we can currently probe. They would need to be large stellar mass objects (since their stellar masses are already large at $z = 0.5$) but have little gas and dust

today. They could plausibly be intermediate-mass ($\log M_* = 10.5$–11.5) early-type galaxies (ETGs) in the local Universe, although they would still be relatively young since they were forming stars actively at $z = 0.4$–0.6. Such depleted objects could have had much more dust in the past with ratios of >4 for the closed box scenario and the model with mantle growth proportional to SFR. In fact, the dust content of such galaxies in the past could be even higher since the build up of a hot X-ray ISM in ETG rapidly destroys any remaining dust (e.g. Jones et al. 1994). This is an attractive solution as severe outflows are then no longer required to reproduce the strong dust mass evolution seen in the DMF. Such a scenario predicts a population of ETGs with moderate dust content and moderate ages (<5–6 Gyr) as the last remnants of their ISM are depleted and the dust gradually destroyed. H-ATLAS has in fact discovered some promising candidates for this transitional phase which are discussed in detail by Rowlands et al. (2011).

Although a closed model does not reproduce the complexity of dust and metal growth within galaxies, we note that this elementary model including mantle growth predicts the *highest* dust masses for galaxies with the same initial gas mass and SFRs. Inflows and outflows of material simply reduce the dust fraction in the ISM. A full treatment of the build up of metals in galaxies from stars of different initial masses further compounds this since relaxing the instantaneous approximation would produce less dust at earlier times (at larger values of f). The difficulties we have in producing the observed dust evolution with this elementary treatment are thus only going to be exacerbated once a more complex treatment is adopted and therefore our conclusions about the requirements for higher yields and condensation efficiencies are conservative. To address the issues above, in particular, the importance of the SF history and the role of the IMF, a more complex model of dust and chemical evolution is required which allows mantle growth, destruction and even the shape of the IMF to depend on the SFR of galaxies. This is beyond the scope of this paper and the reader is referred to Gomez et al. (in preparation) for a more complete investigation of the origin and evolution of dust in galaxies.

6.3 Final caveat

There is one important way in which the observed dust masses could be over-estimated, through the dust mass absorption coefficient κ. This normalizes the amount of emission from dust to the mass of material present and is dependent on the optical properties and shapes of the dust grains (for a more thorough review of the literature, see Alton et al. 2004). The value of κ used here is based on that measured in the diffuse ISM of the Milky Way (Boulanger et al. 1996; Sodroski et al. 1997; Planck Collaboration 2011a) and also on nearby galaxies by James et al. (2002). This value is some 70 per cent higher than that predicted by some models of dust, including the silicate–graphite–PAH model of Li & Draine (2001), but lower than those measured in environments where dust may be aggregated, icy mantles or 'fluffy' (Mathis & Whiffen 1989; Ossenkopf & Henning 1994; Krugel & Siebenmorgen 1994). Latest results from *Planck* (Planck Collaboration 2011a) do see a variation in the dust emissivity with temperature which is expected if there is grain growth in the ISM. It is thus not inconceivable that κ could be globally higher in galaxies with larger fractions of their ISM in states which lend themselves to the growth of grains, or where larger fractions of grains have an SNe origin, or are undergoing destruction by shocks. For example, Ossenkopf & Henning (1994) show that in only 10^5 yr of grain evolution in dense environments (10^6–10^8 cm^{-3}) the dust emissivity can increase by a factor of ∼5 due to the freeze out of molecular ice mantles and coagulation. The same authors also show that changing the ratio of carbon to silicate dust can change the emissivity by ∼40 per cent. Such a change in global dust composition could reflect the time dependence of evolution of various dust sources (e.g. SN-II dominating in early time) or metallicity changes favouring O- or C-rich AGB phases. The mechanism for changing the fraction of the ISM in the densest phases conducive to mantle growth could be triggered SF and feedback (e.g. following an interaction). The fraction of gas in dense clumps has been found to increase markedly in parts of GMCs which are affected by feedback from recently formed OB stars (Moore et al. 2007). Draine et al. (2007) find that for local SINGS galaxies there is no need to consider ice mantles in the modelling of the dust emission, but similar modelling has not been attempted for higher redshift and more sub-mm luminous sources such as the H-ATLAS sources.

A measurement of κ at *Herschel* wavelengths (but for local normal galaxies) has been attempted by Weibe et al. (2009) and Eales et al. (2010b). Both works, however, suggest a much lower value for κ, which would *increase* the dust masses estimated here by a factor of ∼3. Given the already difficult task in modelling the dust masses, we do not believe that κ_{250} can be significantly lower than the values assumed here. A determination of κ for H-ATLAS galaxies is ideally required (as these are *sub-mm selected* sources which may preferentially have higher κ). Should an enhanced κ at higher redshifts be the explanation for the large sub-mm luminosities of H-ATLAS galaxies then this has important implications for the interpretation of all high-z SMG and *Herschel* observations. A change in κ will lead to a change in the opacity of galaxies since the interaction of the grains with optical/UV photons will be altered. A strong test is to look at the effects of different κ on the attenuation–inclination relation in the optical as differing values of κ in the sub-mm will (for a fixed observed sub-mm flux) produce different values for the dust opacity in the optical–UV (see Popescu et al. 2011 for further details). For galaxies in the Millennium Survey (Driver et al. 2007) the Li & Draine (2001) values of κ (which are lower than those used here by 70 per cent) gave the best consistency with the observed attenuation–inclination relation; however it will be interesting to see the results of similar modelling for H-ATLAS sub-mm-selected sources (Andrae et al., in preparation). One result of an increasing κ with redshift would be a flattening of the attenuation–inclination relation with redshift.

A thorough investigation of all the implications using radiative transfer modelling is required but a change in κ is likely to affect dust masses and the outputs of semi-analytic models which try to predict the SMG populations. If the FIR luminosity of high-z galaxies is not dominated by obscured SF (i.e. there is a contribution from low opacity diffuse ISM or 'leaky' star-forming regions) then a change in κ may also lead to a bias in SFR estimated via FIR luminosities. Very high dust masses and sub-mm fluxes for SMG in the early Universe have proved challenging for dust formation models and semi-analytic models of galaxy formation. In addition to exploring additional sources of dust and IMF variations to explain the SMG populations, it is worth considering the possibility of *dust grain property* evolution as well.

7 CONCLUSIONS

We have estimated the DMF for the SDP data from the H-ATLAS survey, and investigated the evolution of the dust mass in galaxies over the past 5 billion years. We find the following.

(i) There is no evidence for evolution of dust temperature out to $z = 0.5$ in this 250 μm selected sample.

(ii) The DMF and dust mass density shows strong evolution out to $z = 0.4$–0.5. In terms of pure mass evolution this corresponds to a factor of 4–5 increase in the dust masses of the most massive galaxies over the past 5 billion years.

(iii) Similar strong evolution is found in the ratio of dust-to-stellar mass and V-band optical depth – *Herschel*-selected galaxies were more dusty and more obscured at $z = 0.4$ compared to today.

(iv) In order to account for the evolution of the dust content we need to radically alter chemical and dust evolution models. We cannot reproduce these trends with Milky Way metal or dust yields or star formation efficiencies.

(v) H-ATLAS 250 μm selected sources are highly efficient at converting metals into dust, either through mantle growth or through a bias in the IMF towards higher mass stars. They must also be observed following an episode of SF (either recent formation or recent major burst) where the gas has been consumed at a much faster rate than galaxies like the Milky Way today.

(vi) As dust and gas (particularly molecular gas associated with SF) are tightly correlated in galaxies, this increase in dust content is suggestive of galaxies being more gas rich at $z = 0.5$. According to the simple chemical model, we are possibly witnessing the period of growth towards peak dust mass when gas fractions are $\sim$0.5 or higher. This strong decline in gas and dust content may be an explanation for the decrease in SFR density in recent times as measured in many multi-wavelength surveys.

This study uses only 3 per cent of the area of the H-ATLAS data. Future improvements will come from the wider area coverage of the full survey, reducing uncertainties due to cosmic variance and small number statistics. Use of deeper optical/IR data from forthcoming surveys such as VISTA-VIKING, pan-STARRS, DES and VST-KIDS will also allow us to push to earlier times and higher redshifts to find the epoch of maximum dust content in the Universe.

ACKNOWLEDGMENTS

HLG acknowledges useful discussions with Mike Edmunds. The H-ATLAS is a project with *Herschel*, which is an ESA space observatory with science instruments provided by European-led Principal Investigator consortia and with important participation from NASA. The H-ATLAS web-site is http://www.h-atlas.org. GAMA is a joint European-Australasian project based around a spectroscopic campaign using the Anglo-Australian Telescope. The GAMA input catalogue is based on data taken from the SDSS and the UKIRT Infrared Deep Sky Survey. Complementary imaging of the GAMA regions is being obtained by a number of independent survey programmes including GALEX MIS, VST KIDS, VISTA VIKING, WISE, H-ATLAS, GMRT and ASKAP providing UV to radio coverage. GAMA is funded by the STFC (UK), the ARC (Australia), the AAO and the participating institutions. The GAMA web-site is http://www.gama-survey.org/. This work received support from the ALMA-CONICYT Fund for the Development of Chilean Astronomy (Project 31090013) and from the Center of Excellence in Astrophysics and Associated Technologies (PBF06).

REFERENCES

Abazajian K. N. et al., 2009, ApJS, 182, 543
Alton P. B., Bianchi S., Rand R. J., Xilouris E. M., Davies J. I., Trewhella M., 1998, ApJ, 507, L125
Alton P. B., Bianchi S., Davies J. I., 1999, A&A, 343, 51
Alton P. B., Xilouris E. M., Misiriotis A., Dasrya K. M., Dumke M., 2004, A&A, 425, 109
Amblard A. et al., 2010, A&A, 518, L9
Baldry I. et al., 2010, MNRAS, 404, 86
Barlow M. et al., 2010, A&A, 518, L138
Baugh C. M. et al., 2005, MNRAS, 356, 1191
Bendo G. et al., 2010, A&A, 518, L65
Bernard J.-A. et al., 2010, A&A, 518, L88
Bianchi S., Schneider R., 2007, MNRAS, 378, 973
Bianchi S., Davies J. I., Alton P. B., 1999, A&A, 344, L1
Blain A. W., Smail I., Ivison R. J., Kneib J.-P., 1999, MNRAS, 303, 632
Boselli A. et al., 2010, A&A, 518, L61
Boulanger F. et al., 1996, A&A, 312, 256
Bourne N. et al., 2011, MNRAS, submitted
Braine J., Guelin M., Dumke M., Brouillet N., Herpin F., Wielebinski R., 1997, A&A, 326, 963
Bruzual G., Charlot S., 2003, MNRAS, 344, 1000
Buat V., Takeuhci T., Burgarella D., Giovannoli E., Murata K. L., 2009, A&A, 507, 693
Burgarella D., Le Floch E., Takeuchi Y., Huang J. S., Buat V., Rieke G. H., Tyler K. D., 2007, MNRAS, 380, 968
Calura F., Pipino A., Matteucci F., 2008, A&A, 479, 669
Calzetti D. et al., 2007, ApJ, 666, 870
Cannon R. et al., 2006, MNRAS, 372, 425
Chabrier G., 2003, PASP, 115, 763
Charlot S., Fall M., 2000, ApJ, 539, 718
Choi P. I. et al., 2006, ApJ, 637, 227
Clements D. L., Dunne L., Eales S. A., 2010, MNRAS, 403, 274
Collister A. A., Lahav O., 2004, PASP, 116, 345
Coppin K. et al., 2008, MNRAS, 384, 1597
Croom S. M. et al., 2009, MNRAS, 392, 19
da Cunha E., Charlot S., Elbaz D., 2008, MNRAS, 388, 1595 (DCE08)
da Cunha E., Eminian C., Charlot S., Blaizot J., 2010a, MNRAS, 403, 1894
da Cunha E., Charmandaris V., Diaz-Santos T., Armus L., Marshall J. A., Elbaz D., 2010b, A&A, 523, 78
Dale D. A., Helou G., Contursi A., Silbermann N. A., Kolhatkar S., 2001, ApJ, 549, 215
Danielson A. L. R. et al., 2011, MNRAS, 410, 1687
Davies J. I., Alton P. B., Bianchi S., Trewhella M., 1998, MNRAS, 300, 1006
Draine B. T. et al., 2007, ApJ, 663, 866
Driver S., Robotham A., 2010, MNRAS, 407, 2131
Driver S., Popescu C. C., Tuffs R. J., Liske J., Graham A. W., Allen P. D., de Propris R., 2007, MNRAS, 379, 1022
Driver S. et al., 2011, MNRAS, 413, 971
Dunne L., Eales S. A., 2001, MNRAS, 327, 697 (DE01)
Dunne L. et al., 2000, MNRAS, 315, 115 (D00)
Dunne L., Eales S. A., Edmunds M. G., 2003a, MNRAS, 341, 589 (DEE03)
Dunne L., Eales S. A., Ivison R. J., Morgan H., Edmunds M. G., 2003b, Nat, 424, 285
Dunne L. et al., 2009, MNRAS, 394, 1307
Dwek E., 1998, ApJ, 501, 643
Dwek E., Cherchneff I., 2011, ApJ, 727, 63
Dwek E., Galliano F., Jones A. P., 2007, ApJ, 662, 927
Dye S. et al., 2010, A&A, 518, L10
Eales S. A., Edmunds M. G., 1996, MNRAS, 299, L29
Eales S. A. et al., 2009, ApJ, 707, 1779
Eales S. et al., 2010a, PASP, 122, 499
Eales S. A. et al., 2010b, A&A, 518, L62
Edmunds M. G., 2001, MNRAS, 328, 223
Edmunds M. G., Eales S. A., 1998, MNRAS, 299, L29
Ferrarotti A. S., Gail H.-P., 2006, A&A, 447, 553
Fukugita M., Peebles P. J. E., 2004, ApJ, 616, 643
Gall C., Andersen A. C., Hjorth J., 2011, A&A, 528, 13
Garn T. et al., 2010, MNRAS, 402, 2017
Gehrz R., 1989, in Allamandola L. J., Tielens A. G. G. M., eds, Proc. IAU Symp. 135, Interstellar Dust. Kluwer, Dordrecht, p. 445
Gomez H. et al., 2009, MNRAS, 397, 1621

Griffin M. et al., 2010, A&A, 518, L3
Gruppioni C. et al., 2010, A&A, 518, L27
Gunawardhana M. et al., 2011, MNRAS, 415, 1647
Harayama Y., Eisenhauer F., Martins F., 2008, ApJ, 675, 1319
Helou G., 1986, ApJ, 311, L33
Hill D. et al., 2011, MNRAS, 412, 765
Hippelein H., Haas M., Tuffs R. J., Lemke D., Stickel M., Klaas U., Volk H. J., 2003, A&A, 407, 137
Hopkins A. M., 2004, ApJ, 615, 209
Huchra J., Davis M., Latham D., Tonry J., 1983, ApJS, 52, 89
Ibar E. et al., 2010, MNRAS, 409, 38
Inoue A. K., 2003, PASJ, 55, 901
James A. et al., 2002, MNRAS, 335, 753
Jones A. P., Tielens A., Hollenbacj D. J., McKee C. F., 1994, ApJ, 433, 797
Jones D. H. et al., 2009, MNRAS, 399, 683
Kennicutt R. C., 1998, ApJ, 498, 541
Kennicutt R. C. et al., 2009, ApJ, 703, 1672
Kramer C. et al., 2010, A&A, 518, L67
Krugel E., Siebenmorgen R., 1994, A&A, 288, 929
Lawrence A. et al., 2007, MNRAS, 379, 1599
Le FLoc'h E. et al., 2005, ApJ, 632, 169
Li A., Draine B. T., 2001, ApJ, 554, 778
Liu G. et al., 2010, AJ, 139, 1190
Madau P., Ferguson H. C., Dickinson M. E., Giavalisco M., Steidel C. C., Fruchter A., 1995, MNRAS, 283, 1388
Mathis J. S., Whiffen G., 1989, ApJ, 341, 808
Meijerink R., Tilanus R. P. J., Dullemond C. P., Israel F. P., van der Werf P. P., 2005, A&A, 430, 427
Ménard B., Scranton R., Fukugita M., Richards G., 2010, MNRAS, 405, 1025
Michałowski M. J., Murphy E. J., Hjorth J., Watson D., Hjorth J., Gall C., Dunlop J. S., 2010, A&A, 522, 15
Moore T. et al., 2007, MNRAS, 379, 663
Morgan H. L., Edmunds M. G., 2003, MNRAS, 343, 427
Morgan H., Dunne L., Eales S. A., Ivison R. J., Edmunds M. G., 2003, ApJ, 597, L33
Negrello M. et al., 2010, Sci, 330, 800
Ossenkopf V., Henning Th., 1994, A&A, 291, 943
Page M. J., Carrera F. J., 2000, MNRAS, 311, 433 (PC00)
Papadopoulos P. P., 2010, ApJ, 720, 226
Papadopoulos P. P., Pelupessy F. I., 2010, ApJ, 717, 1037
Pascale E. et al., 2011, MNRAS, 415, 911
Pilbratt G. et al., 2010, A&A, 518, L1
Planck Collaboration, 2011a, A&A, in press (arXiv:1011.2036)
Planck Collaboration, 2011b, A&A, in press (arXiv:1011.2045)
Poglitsch A. et al., 2010, A&A, 518, L2
Popescu C. C., Tuffs R. J., Volk H. J., Pierini D., Madore B. F., 2002, ApJ, 567, 221
Popescu C. C., Tuffs R. J., Dopita M. A., Fischer J., Kylafis N. D., Madore B. F., 2011, A&A, 527, 109
Pozzetti L. et al., 2007, A&A, 474, 443
Rex M. et al., 2010, A&A, 518, L13
Rho J. et al., 2008, ApJ, 673, 271
Rigby E. E. et al., 2011, MNRAS, 415, 2336
Rowlands K. et al., 2011, MNRAS, submitted
Sargent B. A. et al., 2010, ApJ, 716, 878
Saunders W., Rowan-Robinson M., Lawrence A., Efstathiou G., Kaiser N., Ellis R. S., Frenk C. S., 1990, MNRAS, 242, 318
Saunders W. et al., 2000, MNRAS, 317, 55
Scalo J. M., 1986, Fund. Cosmic Phys., 11, 1
Schechter P., 1976, ApJ, 203, 297
Schmidt M., 1968, ApJ, 151, 393
Serjeant S., Harrison D., 2005, MNRAS, 356, 192
Seymour N., Symeonidis M., Page M. J., Huynh M., Dwelly T., McHardy I., Rieke G., 2010, MNRAS, 402, 2666
Smith D. J. B. et al., 2011a, MNRAS, in press (doi:10.1111/j.1365-2966.2011.18827.x) (arXiv:1007.5260)
Smith D. J. B. et al., 2011b, MNRAS, submitted
Sodroski T. J., Odegard N., Arendt R. G., Dwek E., Weiland J. L., Hauser M. G., Kelsall T., 1997, ApJ, 480, 173
Soifer B. T., Boehmer L., Neugebauer G., Sanders D. B., 1989, AJ, 98, 766
Stevens J. A., Amure M., Gear W. K., 2005, MNRAS, 357, 361
Stickel M., Klaas U., Lemke D., 2007, A&A, 466, 831
Sutherland R., Saunders R., 1992, MNRAS, 259, 413
Swinbank M. et al., 2010, Nat, 464, 733
Symeonidis M., Page M. J., Seymour N., Dwelly T., Coppin K., McHardy I., Rieke G. H., Huynh M., 2009, ApJ, 660, L73
Symeonidis M., Page M. J., Seymour N., 2011, MNRAS, 411, 983
Tielens A. G. G. M., 1998, ApJ, 499, 267
Todini P., Ferrara A., 2001, MNRAS, 325, 726
Tuffs R. J., Popescu C. C., Volk H. J., Kylafis N. D., Dopita M. A., 2004, A&A, 419, 835
VanDalfsen M. L., Harris W. E., 2004, ApJ, 127, 368
Villar V. et al., 2008, ApJ, 677, 169
Vlahakis C., Dunne L., Eales S. A., 2005, MNRAS, 364, 1253 (VDE05)
Wang L., Jing Y. P., 2010, MNRAS, 402, 1796
Wang L., Rowan-Robinson M., 2009, MNRAS, 398, 109
Weibe D. V. et al., 2009, ApJ, 707, 1809
Willmer C. N. A. et al., 2009, ApJ, 138, 146
Xu K. C. et al., 2007, ApJS, 173, 432
Zhukovska S., Gail H.-P., Trieloff M., 2008, A&A, 479, 453

APPENDIX A: CHEMICAL EVOLUTION MODELLING

This simple chemical evolution model describes the star, gas, metal and dust content of a galaxy making the instantaneous recycling approximation. The mass fraction of metals, Z, in this model changes as a mass ds of the ISM is formed into stars assuming no inflows or outflows via the following equation (Edmunds 2001):

$$\mathrm{d}(Zg) = \alpha p \mathrm{d}s + (1-\alpha) Z \mathrm{d}s - Z \mathrm{d}s, \tag{A1}$$

where g is the gas mass and α (equation A2) is the fraction of mass from a generation of SF which is locked up in long-lived stars or remnants m_R as determined by the IMF ($\phi(m)$):

$$\alpha = 1 - \int_{m_1}^{m_2} [m - m_R(m)]\, \phi(m)\, \mathrm{d}m. \tag{A2}$$

p is the effective yield of heavy elements from stars $p = p'/\alpha \sim 0.01$ where $\alpha \sim 0.7$ in agreement with Milky Way values for a Scalo IMF.

In a closed box model (i.e. no inflow or outflow of material), the total mass of the system ($M_{\rm tot}$ = gas + stars) is unity so that the fraction of gas in a galaxy (the ratio of gas mass to total baryonic mass) is $f = g$. In this scenario, the initial conditions are: $Z = 0$ at $g = f = 1$ and the gas mass of the galaxy is given by $g = 1 - \alpha s$. The analytic solution for the metal mass fraction Z is (equation A3)

$$Z = -p \ln f. \tag{A3}$$

An early episode of SF prior to the evolution of the closed box would pre-enrich the gas and increase the interstellar metallicity (pre-enrichment is often invoked to explain the metallicities of globular clusters in the Milky Way). We can include pre-enrichment of the ISM with metals Z_i using

$$Z = Z_i - p \ln f \tag{A4}$$

where $Z_i \sim 0.1$–$0.2\, Z_\odot$ (VanDalfsen & Harris 2004). Correspondingly, the dust mass fraction y varies with ds via:

$$\mathrm{d}(yg) = \alpha p \chi_1 \mathrm{d}s + (1-\alpha)\chi_2 Z \mathrm{d}s - y \mathrm{d}s, \tag{A5}$$

where χ is a parameter to describe the fraction of the mass of interstellar metals in dust grains from SNe remnants or their massive

star progenitors (χ_1), and/or from the stellar atmospheres of LIMS (χ_2). The analytic solution is given in equation (A6) for $y = 0$ at $g = 1$ and for $\alpha = 0.7$ (typical locked up fraction for a Scalo IMF):

$$y = 2.3 \left[\frac{(\chi_1 - \chi_2)\left(1 - f^{0.43}\right)}{\ln(1/f)} + 0.43\chi_2 \right] p \ln(1/\mathrm{f}). \quad \text{(A6)}$$

For the special case where $\chi_1 = \chi_2 = \chi$, equation (A6) reduces to

$$y = \chi p \ln(1/f). \quad \text{(A7)}$$

We can add an additional term to the dust mass from stars by assuming that grains accrete at a rate proportional to the available metals and dust cores in dense interstellar clouds (following Edmunds 2001):

$$y = \chi p \ln(1/g) + \epsilon\eta_c(z - y), \quad \text{(A8)}$$

where ϵ is the fraction of the ISM dense enough for mantle growth (here we set this arbitrarily to 0.3), and η_c is the efficiency of interstellar depletion in the dense cloud (i.e. if all the metals in the dense clouds are accreted on to dust grains then $\eta_c = 1$).

Dust destruction via SN shocks can be added to this elementary model by assuming some fraction δ of interstellar grains are removed from the ISM as a mass ds is forming stars (therefore adding a term $-\delta \mathrm{d}s$ to equation A5). In this work, we test both a constant fraction with $\delta = 0.3$ (appropriate for MW-type galaxies and therefore provides a test case with a minimum destruction level expected for the H-ATLAS spirals) and a function that varies proportionally to the SFR (since a higher SFR equates to a higher Type II SN rate).

Outflow

We include a simple model for outflow of gas, in which gas is added or lost from the system at rates proportional to the SFR. For large galaxies this outflow rate is assumed to be less than four times the SFR ($\lambda/\alpha \leq 4$; see Eales & Edmunds 1996 for discussion; this corresponds to a galaxy which retains only ~ 20 per cent of its original mass). We do not consider inflow of unenriched material since this only slightly reduces the dust mass with respect to the closed box model and does not significantly change the evolution of a galaxy (Edmunds 2001). One can imagine a scenario with inflow of pre-enriched material (e.g. merger), providing new material for SF, even at later times when the original gas mass of the galaxy has been consumed through the SF efficiency parameter k. Modelling the effects of this on the dust mass is beyond the scope of the simple model presented here.

Outflows remove dust from the ISM via $-\lambda y \mathrm{d}s$. The solution is given by equation (A9) if destruction $\delta = 0$:

$$y(\text{outflow}) = \frac{y}{1 + \lambda/\alpha}. \quad \text{(A9)}$$

The gas mass g is related to the gas fraction f in this model by

$$g(\text{outflow}) = \frac{f}{1 + (\lambda/\alpha)(1 - f)}, \quad \text{(A10)}$$

the metallicity mass fraction, Z:

$$Z(\text{outflow}) = -\frac{p \ln(g)}{1 + \lambda/\alpha}, \quad \text{(A11)}$$

and the total mass of the system is

$$M_{\mathrm{tot}}(\text{outflow}) = \frac{1 + (\lambda/\alpha)g}{1 + \lambda/\alpha}. \quad \text{(A12)}$$

Dust and stellar mass

The dust mass per unit stellar mass for the elementary model for equal χ with no mantles, destruction or outflow is given by equation (A13):

$$\frac{M_{\mathrm{d}}}{\alpha s} = \frac{-\chi p g \ln(g)}{1 - g}. \quad \text{(A13)}$$

We can rewrite equation (A13) as a function of time, since SFR $\psi(t)$ is related to the gas mass via

$$\psi(t) = kg(t)^{1.5}, \quad \text{(A14)}$$

where k is the SF efficiency measured in Gyr^{-1} and the variation of g with time is

$$g = \left(\frac{1.5}{\alpha k t + 1.5} \right)^2. \quad \text{(A15)}$$

High values of k will result in a higher SFR and a more rapid build up of the final stellar mass for the same initial gas mass.

For outflow models, the dust mass fraction and the gas mass are reduced as described in equations (A9)–(A11).

This paper has been typeset from a TEX/LATEX file prepared by the author.